Univerzita Karlova v Praze
Přírodovědecká fakulta

Studijní program: Biologie
Studijní obor: Fyziologie živočichů

Bc. Barbora Eliášová

Regulace objemu astrocytů v průběhu stárnutí

Astrocyte volume regulation during aging

Diplomová práce

Vedoucí diplomové práce: Ing. Miroslava Anděrová, CSc.

Praha 2015

Prohlášení:

Prohlašuji, že jsem závěrečnou práci zpracovala samostatně a že jsem uvedla všechny použité informační zdroje a literaturu. Tato práce ani její podstatná část nebyla předložena k získání jiného nebo stejného akademického titulu.

V Praze, 30. 04. 2015

Barbora Eliášová

Poďakovanie:

Chcela by som poďakovať hlavne svojej školiteľke Ing. Miroslave Anděrovej, CSc. za jej odborné vedenie, podnetné pripomienky a trpezlivosť. Takisto ďakujem Mgr. Lenke Harantovej za jej pomoc a ochotu a mojej rodine a priateľom za ich neustálu podporu.

Abstrakt

Astrocyty, ako jeden z druhov gliových buniek, hrajú dôležitú úlohu v zdravo fungujúcej centrálnej nervovej sústave, ale takisto aj v jej patológii. Keďže jedna z ich funkcií je udržiavanie iónovej, neurotransmiterovej a vodnej homeostázy, astrocyty majú schopnosť regulovať svoj objem. Hypo- a hyperosmotický stres môže byť spúšťačom regulatórneho poklesu alebo regulatórneho zväčšenia objemu, vďaka čomu udržujú astrocyty svoj objem stabilný. Počas starnutia prechádzajú astrocyty spolu so zvyškom mozgu rôznymy zmenami. Aby sme určili, či sa tieto zmeny týkajú aj mechanizmov regulujúcich objem, použili sme trojdimenzionálnu morfometriu, ktorá zahŕňa skenovanie fluorescenčne značených astrocytov v mozgových rezoch z EGFP/GFAP myší pomocou konfokálnej mikroskopie a kvantifikáciu ich objemu počas aplikácie rôznych patologických stimulov. Časovo závislé zmeny objemu u hipokampálnych astrocytov boli zaznamenané počas aplikácie hypoosmotického roztoku a roztoku s vysokou koncentráciou draslíka. U štyroch skúmaných vekových skupín boli objavené niekoľké rozdiely v objemových zmenách, spoločne s pár rozdielmi v objeme astrocytov medzi pohlaviami. Podobne ako v predošlých štúdiách, pri použití hypoosmotického roztoku boli identifikované dve subpopulácie astrocytov: astrocyty s nízkou odpoveďou, ktorých objem bol po celý čas stály, a astrocyty s vysokou odpoveďou, ktoré počas aplikácie hypoosmotického roztoku badateľne opúchali.

Kľúčové slová: astrocyty, objemové zmeny, starnutie, EGFP/GFAP myši, 3D morfometria

Abstract

Astrocytes, as one of the glial cell types, have many important functions in healthy functioning of the central nervous system (CNS) but also in its pathology. Since they play a key role in maintenance of ionic, neurotransmitter and water homeostasis in CNS, they possess the ability to regulate their volume. Hypo- or hyperosmotic stress can trigger regulatory volume decrease or increase in astrocytes in order to stabilize their volume. During aging, astrocytes undergo many changes together with the rest of the brain. In order to determine whether these alterations involve also regulatory volume mechanisms, we employed three dimensional morphometry, which comprises confocal microscope scanning of fluorescently labelled astrocytes in brain slices of EGFP/GFAP mice and quantification of astrocyte volume during different pathological stimuli. Time-dependent volume changes of hippocampal astrocytes were recorded while applying either hypoosmotic solution or solution with high extracellular potassium concentration. In the four different age groups studied in the experiment, several differences in volume changes were discovered together with some sex-dependent alterations in astrocyte volume. Additionally, in accordance with previous studies, two subpopulation of astrocytes were identified using hypoosmotic solution: low response astrocytes, with steady volume during whole application, and high response astrocytes, presenting marked swelling during application of hypoosmotic solution.

Key words: astrocytes, volume changes, aging, EGFP/GFAP mice, 3D morphometry

Table of Contents

List of Abbreviations

2D – two dimensional

3D – three dimensional

3M – three month-old

9M – nine month-old

12M – twelve month-old

18M – eighteen month-old

aCSF – artificial cerebrospinal fluid

$aCSF_{H-100}$ – hypoosmotic solution

$aCSF_{K+}$ – solution with high potassium concentration

ALdh1L1 – aldehyde dehydrogenase 1 family, member L1

AMPA – α-amino-3-hydroxy-5-methyl-4-isoxazolepropionic acid

AQP – aquaporin

ATP – adenosine triphosphate

BBB – blood-brain barrier

CA – cornu ammonis

ClC2 – chloride channel 2

CNS – central nervous system

CSF – cerebrospinal fluid

DAPI – 4', 6-diamidino-2-phenylindole

EAAT – excitatory amino-acid transporter

ECS – extracellular space

EGFP – enhanced green fluorescent protein

ER – endoplasmic reticulum

GABA – γ-aminobutyric acid

GFAP – glial fibrillary acid protein

GLAST – glutamate aspartate transporter

GLT1 – glutamate transporter 1

GS – glutamine synthetase

HR – high response

Il-6 – interleukin 6

InsP3 – inositol trisphosphate

K_{2p} – two-pore domain potassium channel

Kir – inwardly rectifying potassium channel

LR – low response

LTP – long-term potentiation

MHCII - major histocompatibility complex class II

NG2 – chondroitin sulphate proteoglycan NG2

NKCC – Na^+ -K^+-Cl^- co-transporter

NMDA – N-methyl D-aspartate

NMDG – N-methyl-D-glucamine

PBS – phosphate-buffered saline

PFA – paraformaldehyde

PTB – sodium-pentobarbital

ROS – reactive oxygen species

RVD – regulatory volume decrease

RVI – regulatory volume increase

S100β - S100 calcium binding protein B

SASP – senescence-associated secretory phenotype

SEM – standard error of the mean

TNFα – tumor necrosis factor α

VRAC – volume-regulated anion channel

Introduction

Astrocytes are the most abundant glial cells in central nervous system. They play crucial role in the development of the central nervous system and its healthy functioning. Additionally, they often determine the response to brain trauma or ischemia (Pekny and Nilsson 2005). Frequently, astrocytes present rapid swelling during traumatic brain injury, implying the importance of the ability to regulate cell volume (Kimelberg 2005). When exposed to hypo- or hyperosmotic stress, astrocytes are capable of regulatory volume decrease or increase through special mechanisms involving number of ion and water channels. However, exact mechanisms of these two processes are still unknown (Benfenati and Ferroni 2010). During aging, entire central nervous system undergoes multiple changes leading mostly to its deterioration. Astrocytes are affected by physiological aging as well and undergo many alterations, most of which still needs to be enlighten (Rodríguez-Arellano et al. 2015). This study aims to characterize age-induced changes in cell volume regulations, using mice expressing enhanced green fluorescent protein under the promoter for human glial fibrillary acid protein as a model of aging and three-dimensional morphometry to determine astrocyte volume.

Astrocytes

The central nervous system (CNS) is composed of two predominant cell types: neurons and glia. Glial cells comprise microglia, oligodendrocytes, polydendrocytes and astrocytes, of which the latest is the most abundant glial cell type. Once considered only some kind of brain glue, today they are well known for many of their functions vital for healthy functioning of the CNS (Simard and Nedergaard 2004).

Basic morphology and anatomical organization

On the basis of differences in their cellular morphologies and anatomical locations, astrocytes are divided into two major subtypes: protoplasmic and fibrous astrocytes. Protoplasmic astroglia are located mainly in grey matter and have a globoid shape with several stem branches giving rise to many fine processes. Generally, they extend between five and eight major processes, each of which ramifies into fine leaflet-like appendages uniformly distributed throughout the grey matter (Bushong et al. 2002; Sofroniew and Vinters 2010). In hippocampus or cortex many of these finely branching processes from a single astrocyte contact several hundred dendrites from multiple neurons and envelope 100 000 or more synapses (Halassa et al. 2007; Nedergaard, Ransom, and Goldman 2003). Fibrous astrocytes are found throughout all white matter and exhibit morphology of many long fibre-like processes. Processes of protoplasmic astrocytes envelop synapses, whereas those of fibrous astrocytes contact nodes of Ranvier. Neighbouring astrocytes of both subtypes form gap junctions between their distal processes and they also make extensive contacts with blood vessels (Sofroniew and Vinters 2010).

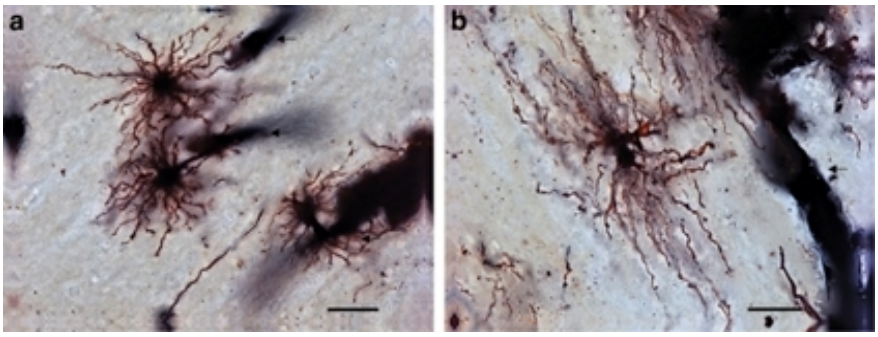

Figure 1: Golgi stained protoplasmic and fibrous astrocytes in the human brain. Protoplasmic astrocytes (a) located in grey matter have spherical cell body and ramified processes radiating in all directions. Fibrous (b) astrocyte found in white matter has more oblong body with long but less branched processes heading predominantly to two opposite directions. Both subtypes are contacting blood vessels (arrows). Scale bar (a): 10 μm; scale bar (b): 25 μm. (Torres-Platas et al. 2011)

The entire CNS is plated with astrocytes in an adjoining and essentially non-overlapping way that is orderly and well organized. There are no CNS regions lacking astrocytes or closely related cells, such as Müller cells of retina or Bergmann glia of the cerebellar cortex. In grey matter, individual protoplasmic astrocytes have essentially non-overlapping domains, however, they do not form unique non-collaborating units. Together they form astrocyte syncytia of various sizes through gap junctions made of specific connexins. These junctions are located on the distant processes, where the fine spongiform branches from individual astrocytes interlink with one another (Bushong et al. 2002; Dermietzel and Spray 1993; Ogata and Kosaka 2002).

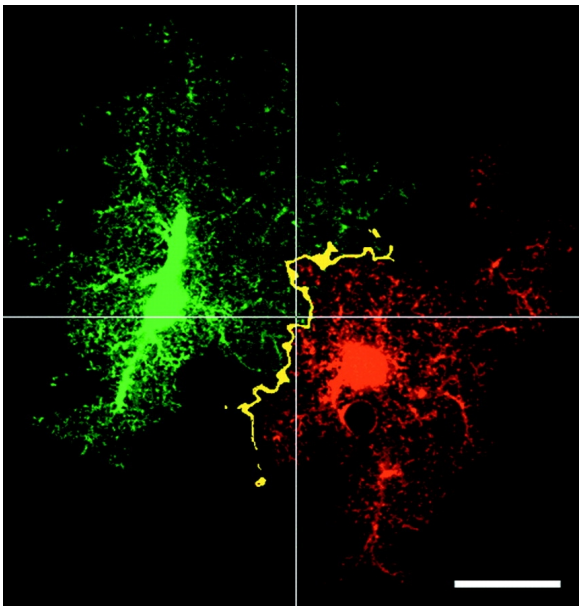

Figure 2: Astrocyte domains overlap. Two protoplasmic astrocytes are filled with distinct fluorescent dyes. Pixels containing both green and red colour are pseudo-coloured yellow, marking the overlapping area where the fine processes of both astrocytes interact. Scale bar, 20µm. (Bushong et al. 2002)

Astrocyte domains can be distinguished both in humans and rodents (Bushong et al. 2002; Oberheim et al. 2009; Ogata and Kosaka 2002), but the overlapping areas are greater and more common in human brain, suggesting higher degree of coupling. It is also noteworthy that human cortical astrocytes are larger, and structurally both more complex and more diverse, than those of rodents. This is implying that the complexity and size of astroglia increases with the evolution of CNS and the rising intellect (Oberheim et al. 2009). In white matter, similar individual astrocyte domains appear likely to exist, but this notion has yet to be examined (Sofroniew and Vinters 2010).

Molecular markers

A prototypical marker for immunohistochemical identification of astrocytes is expression of glial fibrillary acid protein (GFAP). It belongs to a family of intermediate filament proteins (including vimentin, nestin, and others) that fulfil cyto-architectural functions. Studies in transgenic mice that do not express GFAP suggest that in healthy CNS, GFAP is not essential for the normal appearance and function of most astrocytes, however it is crucial in the process of reactive astrogliosis and glial scar forming (Pekny and Pekna 2004). At the single-cell level, GFAP cytoskeleton is present mainly in primary branches radiating out of the central hub, which is sometimes composed of a triangular structure within the soma of the astrocyte. It is completely absent from the fine spongiform processes (Bushong et al. 2002). Nevertheless, one must be aware of its limitations in use as an astrocyte marker. Immunohistochemically, GFAP was first associated with reactive astrocytes in old demyelinated plaques from multiple sclerosis patients and other pathological contexts. Since then, GFAP expression can be regarded as a reliable marker that labels most reactive astrocytes. However, it is not an absolute marker of all non-reactive astrocytes as certain subpopulation of astrocytes in healthy CNS does not express detectable levels of GFAP (Eng, Ghirnikar, and Lee 2000).

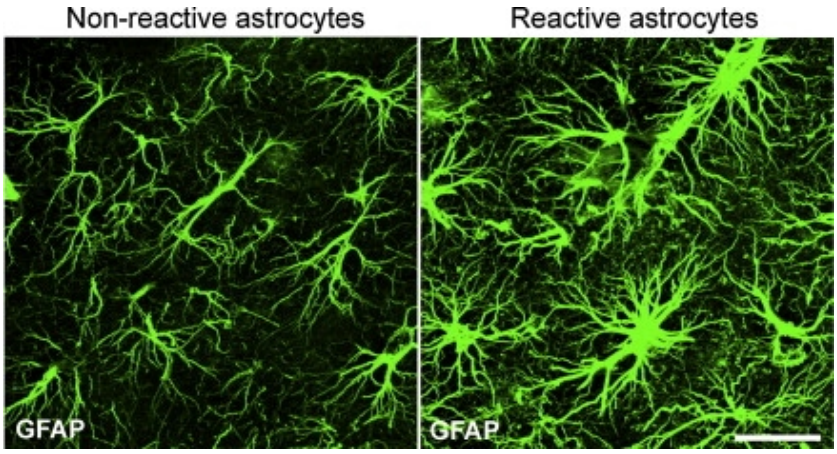

Figure 3: Immunodetection of astrocyte GFAP in mouse hippocampus. Reactive astrocytes show greater GFAP immunoreactivity than the nonreactive astrocytes. Scale bar: 25μm. GFAP – glial fibrillary acid protein. (Pekny, Wilhelmsson, and Pekna 2014)

In addition, there are other molecular markers that have been used for immunohistochemical identification of astroglia including glutamine synthetase (GS) or S100 calcium binding protein B (S100β) (Gonçalves, Leite, and Nardin 2008; Norenberg 1979). Promising candidate for a reliable astrocyte molecular marker is aldehyde dehydrogenase 1

family, member L1 (ALdh1L1) protein. It was identified as a highly specific antigenic marker for astrocytes with an extensively broader pattern of astrocyte expression than the traditional GFAP (Barres 2008).

Development of CNS and astrocytes

Astrocytes not only provide a number of important functions in the adult CNS, but they are essential also for its healthy development. Astroglia create molecular boundaries in the extracellular matrix, which take part in guiding the migration of developing axons (Powell and Geller 1999). They participate in the formation of developing synapses and they support their functioning (Barres 2008; Ullian et al. 2001). In addition, astrocytes appear to also influence developmental elimination of synapses (Stevens et al. 2007). Furthermore, these glial cells play a role in the development of white matter: the loss or dysfunction of their connexins and gap junctions leads to demyelination (Lutz et al. 2009).

Signalling within astroglial syncytium

As mentioned before, astrocytes are not physically separated cells as neurons, they are integrated into continuous structures known as astroglial syncytia through the gap junctions located on the distant processes. These gap junctions are formed by intracellular channels – connexons, creating a pore between two cells, which is permeable to molecules of molecular weight approximately 1KDa and is involved in long-range glial signalling (Dermietzel and Spray 1993; Giaume and Venance 1998; Verkhratsky et al. 2010).

Even though astrocytes are unable to generate propagating action potentials (Verkhratsky et al. 2010) they are still able of long-range signalling. One of the signalling pathways is through calcium (Ca^{2+}) waves. Calcium, stored in endoplasmic reticulum (ER), is released upon a corresponding signal, for example upon activation of metabotropic G protein-coupled receptors. Activation of these receptors leads to formation of second messenger molecule inositol trisphosphate (InsP3) triggering the Ca^{2+} release. This is the predominant pathway in astrocyte signalling. After Ca^{2+} efflux from the ER, signal is capable of propagating through glial syncytium using several complimentary mechanisms that include diffusion of InsP3 through gap junctions, or release and extracellular diffusion of gliotransmitters (Cornell-Bell et al. 1990; Scemes and Giaume 2006; Verkhratsky et al. 2010).

Propagating glial Ca^{2+} waves are the most investigated mechanism of long-range glial signalling. However, many other molecules (e.g., metabolic substrates, adenosine

triphosphate, or other second messengers) can alternatively participate in inter-glial signalling systems (Heneka, Rodríguez, and Verkhratsky 2010; Verkhratsky et al. 2010).

CNS metabolism

Astrocytes have a crucial function in the formation and the maintenance of blood-brain barrier (Abbott, Rönnbäck, and Hansson 2006). Many of the astroglial processes form an endfeet embracing brain capillaries thus establishing neuronal-glial-vascular unit integrating neural circuitry with local blood flow. They have multiple bidirectional interactions with blood vessels, including regulation of local blood flow (Oberheim et al. 2009; Sofroniew and Vinters 2010).

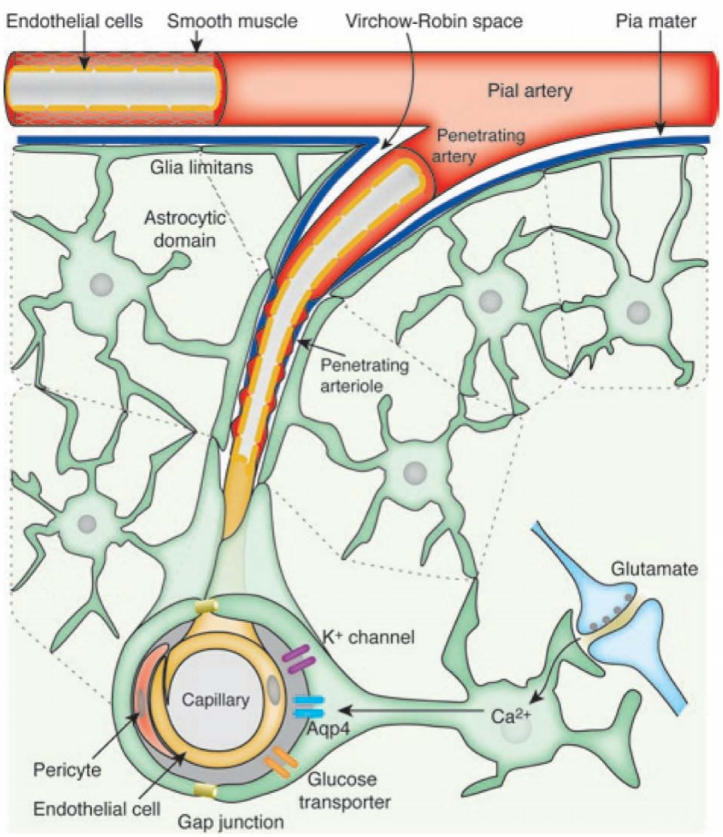

Figure 4: Astrocytes as a part of blood-brain barrier. Astrocyte endfeet enveloping penetrating capillaries express specialized channels, e.g. aquaporin 4 (Aqp4) or certain K^+ channels. Spreading Ca^{2+} waves caused by glutamergic synapse activity may trigger dilatation of the embraced capillary. (Iadecola and Nedergaard 2007)

In response to increased neuronal activity, astrocytes are able to trigger vasodilatation. For example at glutamergic synapses, glutamate binding to astroglial receptors provokes Ca^{2+} oscillations that cause release of vasoactive substances, such as prostaglandins (Zonta et al. 2003). This way, astrocytes are able to regulate the blood flow according to neuronal needs.

Although some of the studies imply that Ca^{2+} waves work also the opposite way and initiate e.g. release of noradrenaline generating vasoconstriction (Iadecola and Nedergaard 2007; Mulligan and Macvicar 2004; Zonta et al. 2003).

By forming the neuronal-glial-vascular unit, astrocytes provide energetic and metabolic support for neurons. About 50% of glucose entering the brain tissue is accumulated in astrocytes in the form of glycogen supplies. These are used in case of hypoglycaemia or during periods of increased neuronal activity through glucose-lactate shuttle operative between astroglia and neurons. An increase in neuronal activity results in an increase of glutamate that is transported into astrocytes along with sodium (Na^+). Rising Na^+ concentration in cytosol stimulates glycolysis that produces lactate, which is then transported to neurons providing them with required energy (Aubert et al. 2007; Brown and Ransom 2007). Additionally, glucose metabolites can be passed across gap junctions thus always providing energy where it is needed (Rouach et al. 2008). Also during hypoglycaemia, astrocyte glycogen breaks down to lactate that is transported to the neighbouring neural elements – both synapses in grey matter and axons in white matter (Brown and Ransom 2007).

The tripartite synapse

Nowadays, it is well known that synapses are not comprised by neurons only, but in fact, they are formed by three elements: by the pre- and postsynaptic neuronal components and by the astroglial perisynaptic processes. This system is generally called a tripartite synapse (Swanson et al. 1999).

Astrocytes express various neurotransmitter receptors, both ionotropic and metabotropic. Activation of these receptors leads mostly to changes in Ca^{2+} concentrations and their stimulation provides the information input to neuroglial circuitry (Verkhratsky and Kettenmann 1996; Verkhratsky and Steinhauser 2000). Expression of these receptors on astrocytes *in vivo* is definitely not random, it is strictly controlled and differs in various CNS regions, e.g. expression of purinergic P2X receptors is frequent in cortical astrocytes but absent in those of hippocampus. These expression patterns are given by immediate neurotransmitter environment and consequently astrocytes are equipped to respond to neurotransmitters released in their domains (Jabs et al. 2007; Lalo et al. 2008; Verkhratsky et al. 2010).

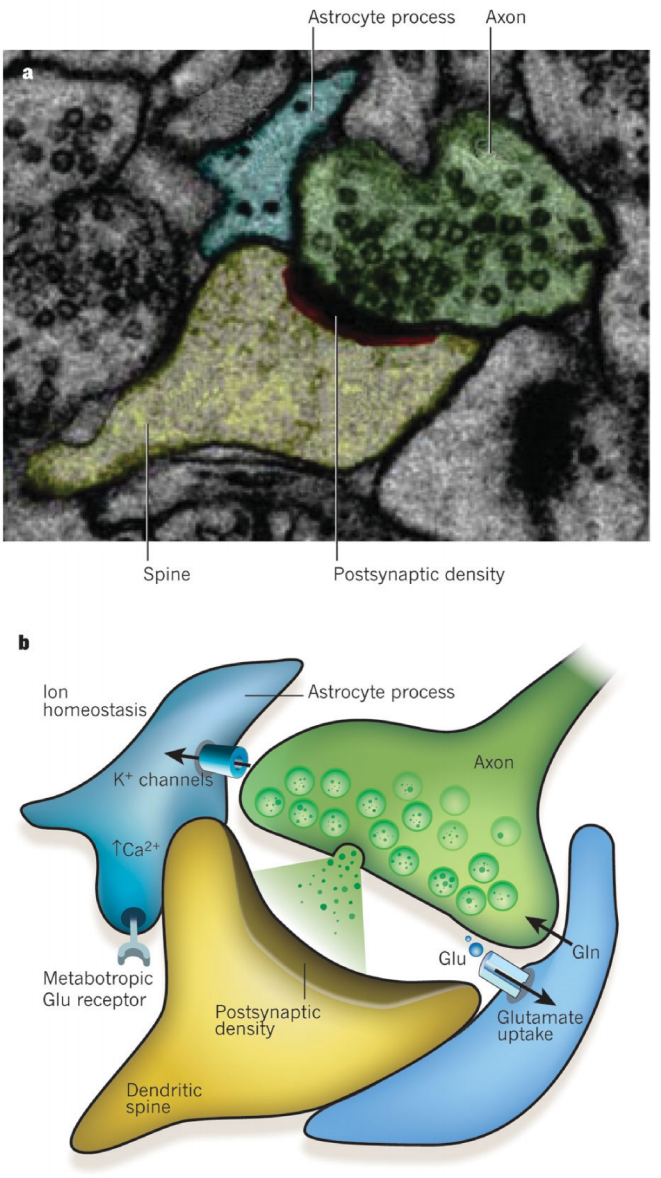

Figure 5: The tripartite synapse. Electron micrograph (a) of cells located in the intact perfusion-fixed rat hippocampus shows tripartite synapse constituted of astrocyte process (blue), axon (green) and dendritic spine (yellow). Schematic representation (b) indicates some of the main functions of astrocyte in the tripartite synapse: maintenance of ion homeostasis, especially by regulating K^+ extracellular levels, and glutamate (Glu) uptake and its conversion to glutamine (Gln), which is later transported back to neurons. Activated astrocyte metabotropic glutamate receptors induce a rise of intracellular Ca^{2+} concentration. (Eroglu and Barres 2010)

Astrocytes have dual role in synapses. They not only can sense the released neurotransmitters but are also able to produce their own so called gliotransmitters and hence modulate the efficacy of synapse. Astroglia are capable of influencing synaptic transmission e.g. by activating N-methyl D-aspartate (NMDA) or adenosine receptors on neurons (Parpura et al. 1994; Pascual et al. 2005) and likewise is important their ability to synchronize neuronal activity through glutamate release (Fellin et al. 2004). Gliotransmission is initiated by changes

in neuronal activity and depends on intracellular Ca^{2+} levels (Halassa, Fellin, and Haydon 2007). Astrocyte transmitters, such as glutamate, adenosine triphosphate (ATP), γ-aminobutyric acid (GABA) or taurine, are released via various ways, e.g. diffusion through large pore channels, through transporters, antiporters or by exocytosis (Heneka, Rodríguez, and Verkhratsky 2010).

CNS homeostasis

In addition to above described functions, astrocytes are necessary for maintaining ionic, neurotransmitter and water homeostasis (Simard and Nedergaard 2004). Proper regulation of the extracellular levels of ions, metabolites and neuroactive molecules is of paramount importance for CNS function.

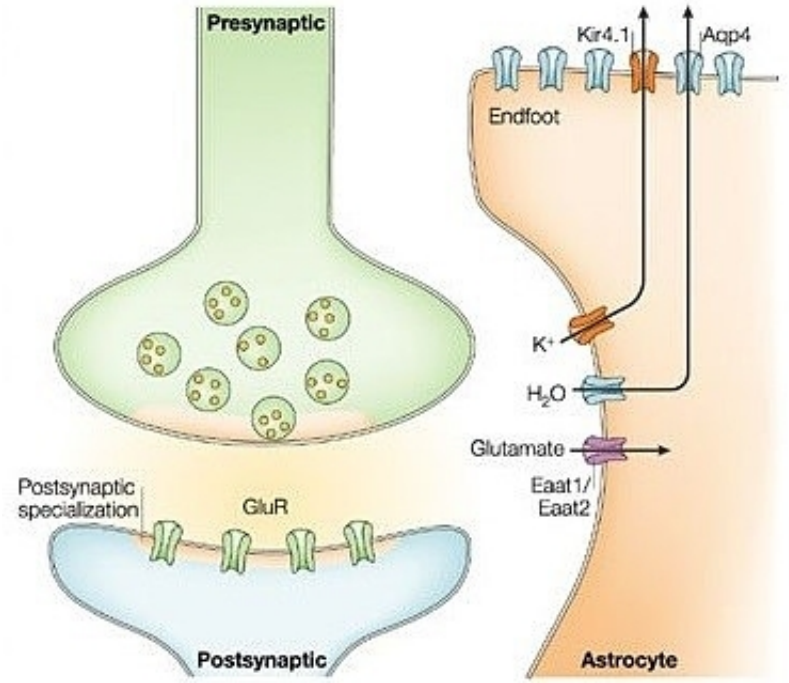

Figure 6: Ion, water and neurotransmitter homeostasis. Schematic layout of simplified glutamergic synapse indicating astrocyte role in maintaining homeostasis of ions (K^+), water (H_2O) and glutamate. Aqp4 – aquaporin 4; Eaat1/Eaat2 – excitatory amino-acid transporter 1/excitatory amino-acid transporter 2; GluR – glutamate receptors; Kir4.1 – inwardly rectifying K^+ channel 4.1. (Amiry-Moghaddam and Ottersen 2003)

Glutamate

Astrocytes play a key role in metabolism of some neurotransmitters, most importantly glutamate. Despite glutamate being the main excitatory neurotransmitter in the CNS, it is also the most powerful neurotoxin. Hence, glutamate levels must be strictly under control as every excess in the extracellular space (ECS) triggers neuronal death. About only 20% of glutamate released during synaptic transmission is accumulated into postsynaptic neurons. Residual

80% must be taken up by astrocytes. This glutamate bulk is then converted by GS, an ATP-dependent glia-specific enzyme, to non-toxic glutamine, which can be safely transported back to the presynaptic neuronal terminal through the ECS (Heneka, Rodríguez, and Verkhratsky 2010). Additionally, glutamate can be transformed by glutamate dehydrogenase to α-ketoglutarate, which is then metabolized and reduced to lactate. Both glutamine and lactate are later used by neurons (Danbolt 2001). Astrocyte glutamate transporters are essential for normal synaptic activity and plasticity. Glutamate uptake is mediated by two different systems: Na^+ independent, comprising mainly chloride (Cl^-) dependent glutamate/cysteine antiporters and representing only a small portion of glutamate uptake; and Na^+ dependent uptake. These are human excitatory amino-acid transporter 1 (EAAT1) and EAAT2; and rodent homologues glutamate aspartate transporter (GLAST) and glutamate transporter 1 (GLT1) (Anderson and Swanson 2000; Pines et al. 1992; Storck et al. 1992).

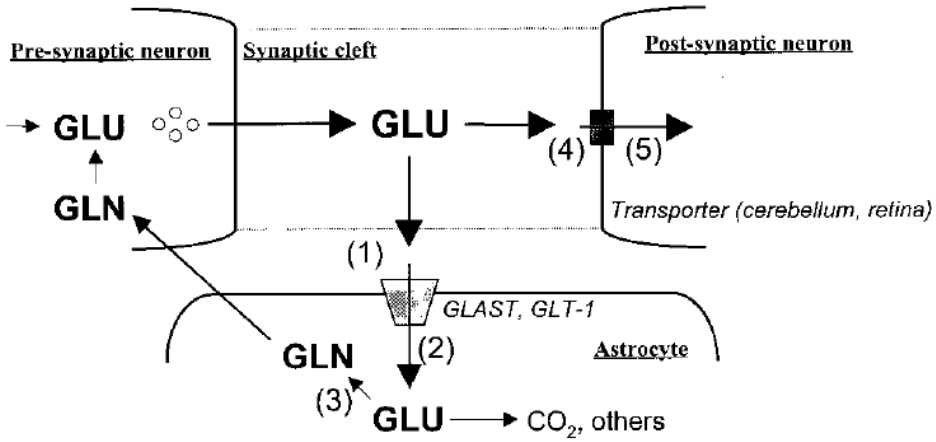

Figure 7: Fate of glutamate released at glutamergic synapses. After being released, most of the glutamate molecules escapes synaptic cleft (dotted line) and binds to (1) glutamate transporters, where they are transported into the astrocyte (2). Inside, glutamate is converted to glutamine (3), which is later transported back to neurons to be reused for glutamate synthesis. Some portion of glutamate molecules (about 20% of glutamate in cerebellar and retinal synapses) binds (4) to neuronal glutamate transporters and is transported into the post-synaptic neuron. GLU – glutamate; GLN – glutamine, GLAST – glutamate aspartate transporter, GLT-1 – glutamate transporter 1. (Anderson and Swanson 2000)

Transport of glutamate against its concentration gradient is realized by coupling its movement with transport of Na^+ ions inside and potassium (K^+) ions outside of the cell, down their respective gradients maintained by Na^+/K^+ ATPases. Transport of one molecule of glutamate requires three Na^+ ions and one K^+ ion and in addition, there is a flow of hydrogen (H^+) ions inside the cell. In the case of severe ATP depletion, glutamate transporters are able

of reverse movement of the substrate causing glutamate leak from astrocytes (Anderson and Swanson 2000).

Potassium

Of particular importance is the maintenance of extracellular K^+ levels that are very low in comparison with its intracellular levels. The K^+ concentrations change during various processes, e.g. its extracellular accumulation accompanies the repolarization phase of action potentials. Astrocytes adopt two regulatory mechanism: K^+ uptake and K^+ spatial buffering (Kofuji and Newman 2004).

In case of K^+ uptake, the excess K^+ ions are temporarily accumulated into glial cells by transporters or K^+ channels and eventually, they are released back into ECS. K^+ ions are always accompanied by anions, such as Cl^-, to preserve electroneutrality, or the uptake is coupled with efflux of another cation, such as Na^+. Accumulation of K^+ ions in astrocytes is accompanied by water influx, which leads to their swelling. Net K^+ uptake is mediated mainly by Na^+/K^+ ATPase pumps (sodium pumps) and Na^+–K^+–Cl^- co-transporters (NKCCs) (Kofuji and Newman 2004). Sodium pump, using the energy from ATP hydrolysis, is responsible for active transport of Na^+ and K^+ ions through the plasma membrane. Each cycle takes two ions of K^+ into the cells and expels three Na^+ ions out of the cell thus maintaining high K^+ levels on the inside of the cell and low on the outside (Kaplan 2002). NKCCs belong to membrane proteins that transport usually one Na^+, one K^+ and two Cl^- ions in or out of the cell depending on the gradient (Haas and Forbush 1998). Several experiments support the notion that sodium pumps are important in K^+ uptake (Ambrosio et al. 2002; Ballanyi, Grafe, and Bruggencate 1987; Ransom, Ransom, and Sontheimer 2000) and at least one isoform of NKCCs is involved in this uptake (Macvicar et al. 2002).

Spatial buffering differs from K^+ uptake in many ways. In this process, astroglial syncytia are involved transferring K^+ ions from regions with high extracellular concentration to those with low concentration. Therefore, ions are not accumulated in the cell and there is no water influx and consequent swelling (even though the water transport is present and will be discussed later).

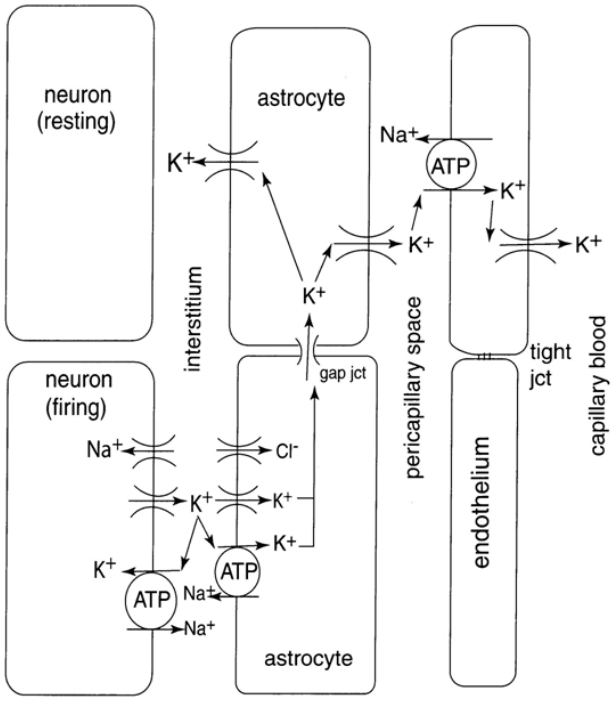

Figure 8: Spatial buffering. K^+ ions are released from neurons through voltage-gated channels and are later recaptured by Na^+/K^+ ATPases located either on neuron itself or on astrocytes, where other K^+ channels participate in the uptake. Together with K^+ ions, Cl^- ions are transported into astrocytes in order to preserve charge balance. K^+ is then redistributed trough astrocyte syncytia to the places where its concentration is low or is taken into the blood flow. (Somjen 2004)

K^+ spatial buffering is possible due to the astrocyte capability to form functional syncytium, where K^+ currents are free to pass and also because of the high and selective K^+ permeability of the astroglial membranes (Kofuji and Newman 2004). The membranes are covered with inwardly rectifying K^+ channels (Kir), which have been described in many CNS regions (Kofuji and Newman 2004). These channels have a high probability of open state at resting potential and allow K^+ ions to flow much more readily in the inward than outward direction (Doupnik, Davidson, and Lester 1995). K^+ flow through the glial network is driven by the difference between glial syncytium membrane potential and the local K^+ equilibrium potential and it is redistributed as needed (Kofuji and Newman 2004).

Water

Every transport or accumulation of ions is necessarily accompanied by water movement. Water homeostasis is also maintained by astrocytes and it is of major importance in a number of physiological processes, not only to compensate the osmolarity changes during ion transports but also in cerebrospinal fluid (CSF) production or cell volume regulation (Nielsen et al. 1997).

Water is transported across astrocyte membranes and redistributed through the syncytium. It enters and leaves the cells through aquaporin channels (Heneka, Rodríguez, and Verkhratsky 2010). Aquaporins (AQP) comprise a family of membrane channels that are water-selective. They can be found in animals, plants and also microorganisms. General structure of AQP is a single polypeptide chain that spans the membrane six times while the loops are creating the pore as so called hour-glass model. AQP assembles in tetramers and each monomer forms functional pore with approximately the diameter of a water molecule (Knepper 1994). Each type of AQP can be distinguished, e.g. by its location and other specializations. In this manner, AQP1 can be found in the brain but is only abundant in choroid plexus, whereas AQP4 is located all over CNS (Jung et al. 1994; Nielsen et al. 1997), predominantly in the membrane of astrocytes.

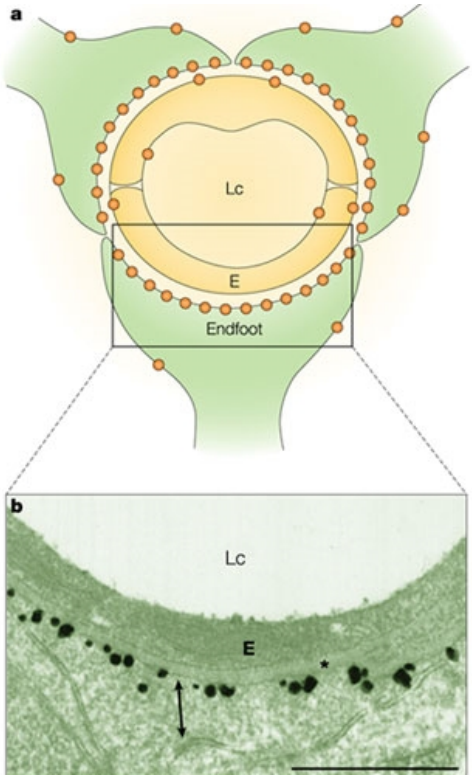

Figure 9: Localization of aquaporin 4 at the blood-brain interface. Schematic layout (a) shows the high concentration of aquaporin 4 (AQP4; orange dots) at the astrocyte perivascular endfeet facing the blood vessel. AQP4 levels drop once the astrocyte membrane loses contact with the basal lamina. Endothelial cells express APQ4 as well but at much lower concentrations. Strong immunogold labelling of astrocyte AQP4 at the perivascular endfeet is seen at the electron micrograph (b). Scale bar: 0.5µm. * - basal lamina, arrow – two membrane domains of the endfoot; E – endothelium, Lc – capillary lumen, (Amiry-Moghaddam and Ottersen 2003)

Concentration of AQP4 is selective, not only in terms of tissue, but also at astrocyte membrane. Not surprisingly, highest amounts are found at the membrane domains facing blood vessels and pia. Lower levels are at the rest of glial membrane, with enrichments at areas enwrapping certain synapses (Nielsen et al. 1997). Higher AQP4 concentrations are found also at the endfeet of astrocytes, and there is a co-localization with Kir channels, suggesting conjugation of K^+ spatial buffering with water fluxes. This way, water is transported from active neuronal synapses to other places, such as subarachnoid space or to blood, and the ECS is reduced (Amiry-Moghaddam and Ottersen 2003; Simard and Nedergaard 2004).

Cell volume regulation

Cell volume is determined by the cellular content of osmotic active compounds and by the extracellular tonicity. With a few exceptions, animal cell membrane is well permeable to water; this permeability is far greater than the permeability towards ions such as Na^+, K^+ or Cl^-. In many cell types, astrocytes including, water permeability is additionally increased by the presence of AQP that leads to the enhanced rate of initial swelling following hypotonic stress (Hoffmann, Lambert, and Pedersen 2009).

A shift in extra or intracellular osmolarity results in the cell volume perturbations. Most cells are able to counteract this distress in order to avoid excessive alterations. In general, they respond to the swelling by a release of KCl, nonessential organic osmolytes, and cell water and therefore reducing their volume towards the original value. This process is called the regulatory volume decrease (RVD). In contrary, a net gain of KCl and water is initiated in osmotically shrunken cells in order to regain the original volume. This is known as the regulatory volume increase (RVI). The normal osmolarity of the extracellular fluid is 285 mosmol/kgH2O and is kept constant under physiological conditions. Hence, most of the volume perturbations are caused by changes in intracellular osmolarity, occurring e.g. during accumulation of nutrients and metabolic waste products. However, also changes in extracellular osmolarity may appear during normal physiological conditions. Additionally, variety of pathophysiological conditions, such as an increase in the extracellular K^+ concentration or hypoxia, presents a challenge to the cell volume regulation (Hoffmann, Lambert, and Pedersen 2009; Lang et al. 1998).

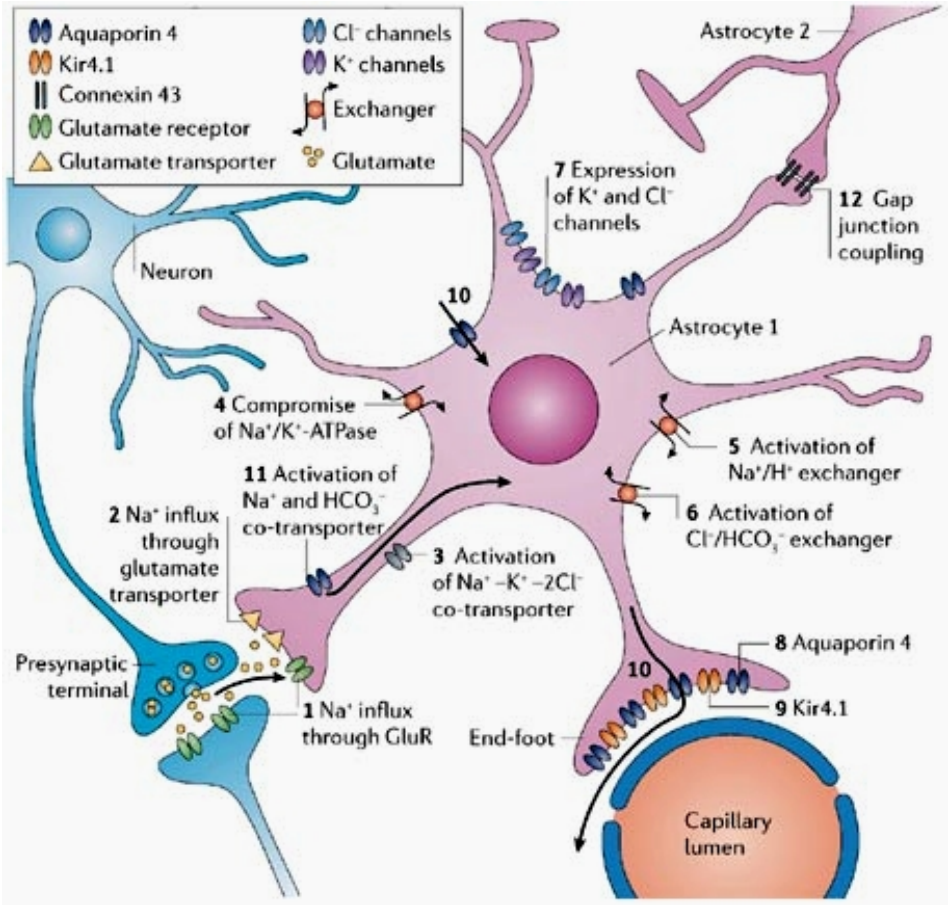

Figure 10: Astrocyte swelling. At glutamergic synapses, neuronal swelling is caused predominantly by influx of Na^+ trough glutamate receptors (GluR) (1). Na^+ influx drives astrocyte glutamate transporters (2), therefore is responsible for glial swelling as well. Higher concentration of K^+ in extracellular space contributes to glial swelling by activation of Na^+-K^+-Cl^- co-transporters (3). Astrocyte Na^+/K^+ ATPases are compromised (4) and various exchangers are activated, e. g. Na^+/H^+ exchanger (5) or Cl^-/HCO_3^- exchanger (6), increasing the astrocyte swelling rate. Astrocytes express many specific channels for K^+ and Cl^- ions (7) and also for water; expression of aquaporin 4 (AQP4) (8) suggest an astrocyte-specific mechanism in oedema formation. Co-localization of AQP4 with inwardly rectifying K^+ channels (Kir4.1) (9) imply its role in spatial buffering. Depolarization of astrocyte caused by extracellular K^+ concentration rise leads to activation of Na^+-HCO_3^- co-transporter (11). As a result, intracellular osmolarity increases driving water inside trough AQPs. Gap junctions (12) between astrocytes ensure water and ion fluxes. (Seifert, Schilling, and Steinhäuser 2006)

Astrocytes, being the main tool of regulation of brain homeostasis, are very sensitive to changes in extracellular osmolarity. In response to decreased osmolarity, astroglia exhibit rapid prominent swelling, followed by returning to original volume. Similarly to the other cells, astrocytes achieve RVD as an active process by a leak of intracellular osmolytes, such as K^+ and Cl^- and some organic molecules. Ions are extruded mainly through volume-sensitive potassium and chloride/anion channels. Water naturally accompanies their movement through AQP4 (Kimelberg 2005; Simard and Nedergaard 2004). Likewise, an

intracellular osmolarity increase is responsible for astrocyte swelling. Water is osmotically forced to influx either via AQPs or via ion co-transporters (Benesova et al. 2009; MacAulay, Hamann, and Zeuthen 2004). There are several reasons for the increase in the intracellular osmolarity. Inhibition of Na^+/K^+-ATPase because of energy depletion during pathological state is one of them. Its dysfunction leads to an influx of osmolytes, such as KCl, followed by water. In addition, energy substrate deprivation together with lack of oxygen influences ECS, where it leads to the accumulation of ions and neurotransmitters, such as glutamate. These interact with astroglia receptors and ion channels, activating cell swelling. Additionally, intra- but also extracellular acidification of various reasons or high concentrations of arachidonic acid trigger astrocyte swelling (Benesova et al. 2009; Kimelberg 2005).

Several studies support the idea that predominantly the astrocyte processes contribute to cell swelling. This is in agreement with the expression pattern of AQP4, which is localised mainly on astrocyte processes, together with certain ion channels and co-transporters, such as Kir channels (Benesova et al. 2009, 2012). Swelling of the processes is accompanied by the increase in the cell complexity. The astrocyte morphology is changing in a complex way, different compartments are not only swelling, but also shrinking and a structural rearrangement occurs (Chvatal et al. 2007).

Generally, perturbations in the cell volume are quickly followed by the regulatory mechanisms. NKCCs are responsible for the process of RVI, through the influx of Na^+, K^+ and Cl^- ions accompanied by water. Increased NKCC activity, e.g. because of ischemia, is however harmful and leads to excessive cell swelling contributing to brain oedema. Other RVI pathways also comprise sodium influx, e.g. Na^+/H^+ exchanger working together with Cl^-/HCO_3 exchanger. In order to save the energy, ion efflux pathways are generally inhibited during RVI (Kahle et al. 2009). RVD can be summarized in three steps: first, the cell swelling take place because of water influx by passive diffusion and through the water channels. Secondly, swollen astrocytes sensing volume changes triggers a chain of biochemical reactions aimed at regulating cell volume. Finally, the release of organic and inorganic osmolytes and water is promoted by the effector mechanism of osmotransduction (Benfenati and Ferroni 2010). Again, co-transporters are involved, in this case it is the K^+-Cl^- co-transporter that play an important role (Ringel and Plesnila 2008). Ion channels involved in RVD are very hard to identify *in vivo*. However, in vitro experiments proved that volume regulated anion channels (VRACs) have a key role in astroglia response to swelling. Other engaged channels are inwardly rectifying Cl^- channels and channels mediating K^+ efflux,

presumably the two-pore domain K^+ channels (K_{2P}) and Kir channels. Astrocyte swelling activates VRACs that not only promote transmembrane fluxes of inorganic anions but also facilitate the flow of small, osmotically active organic molecules, such as taurine, glutamate, aspartate or ATP, endorsing RVD even more (Benesova et al. 2012; Benfenati and Ferroni 2010; Kimelberg, Macvicar, and Sontheimer 2006).

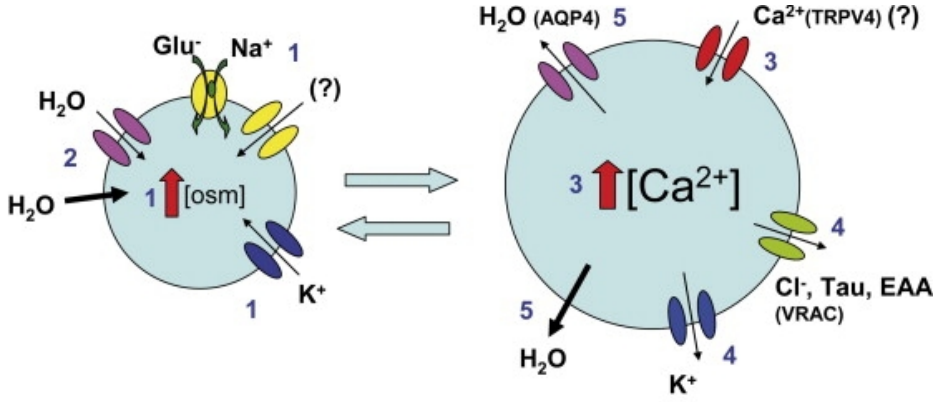

Figure 11: Astrocyte volume regulation. Glutamate, Na^+ and K^+ uptake increases intracellular osmolyte concentration (1), which is in turn driving water inside the cell either through aquaporins or by passive diffusion (2). Intracellular Ca^{2+} concentration rises in response to cell swelling and might be involved in mechanism of osmotransduction together with transient receptor potential cation channel subfamily V member 4 (TRPV4) (3). After the regulatory volume decrease is induced, ions and other osmolytes start to efflux from the cell, accompanied by water (5). Cl^- is getting out trough volume regulated anion channels (VRAC) together with organic osmolytes, like taurine (Tau) or excitatory amino acids (EAA) (4). (Benfenati and Ferroni 2010)

Exact mechanisms involved in astrocyte RVD are still not definitely clear. They differ within at least two astrocyte populations. There are high-response (HR) and low-response (LR) astrocytes. When the swelling occurs, LR cells do not show significant increase of cell volume; in opposite, HR do not present RVD mechanism almost at all, hence the volume increase is higher. Expressed as a fraction of the total cell volume, soma volume is increasing in LR astroglia during hypotonic stress similarly to the volume of the processes. In contrary, soma of HR astrocytes is decreasing in volume, hence it is the volume of the processes that is contributing to the majority of the cell swelling (Benesova et al. 2009; Chvatal, Anderova, and Kirchhoff 2007). These two astrocyte populations have different channel expression and differences in GFAP and taurine levels promoting the variations in volume regulation. Significant alterations are concerning family of K_{2P} channels, but also chloride channels, such as chloride channel 2 (ClC2). It is expressed only by LR astrocytes, presumably supporting their increased ability to regulate the volume. Moreover, the different environments occupied by single astrocytes must be taken into account. Diverse extracellular K^+ and neurotransmitter

concentrations may trigger different volume regulation mechanism (Benesova et al. 2009, 2012).

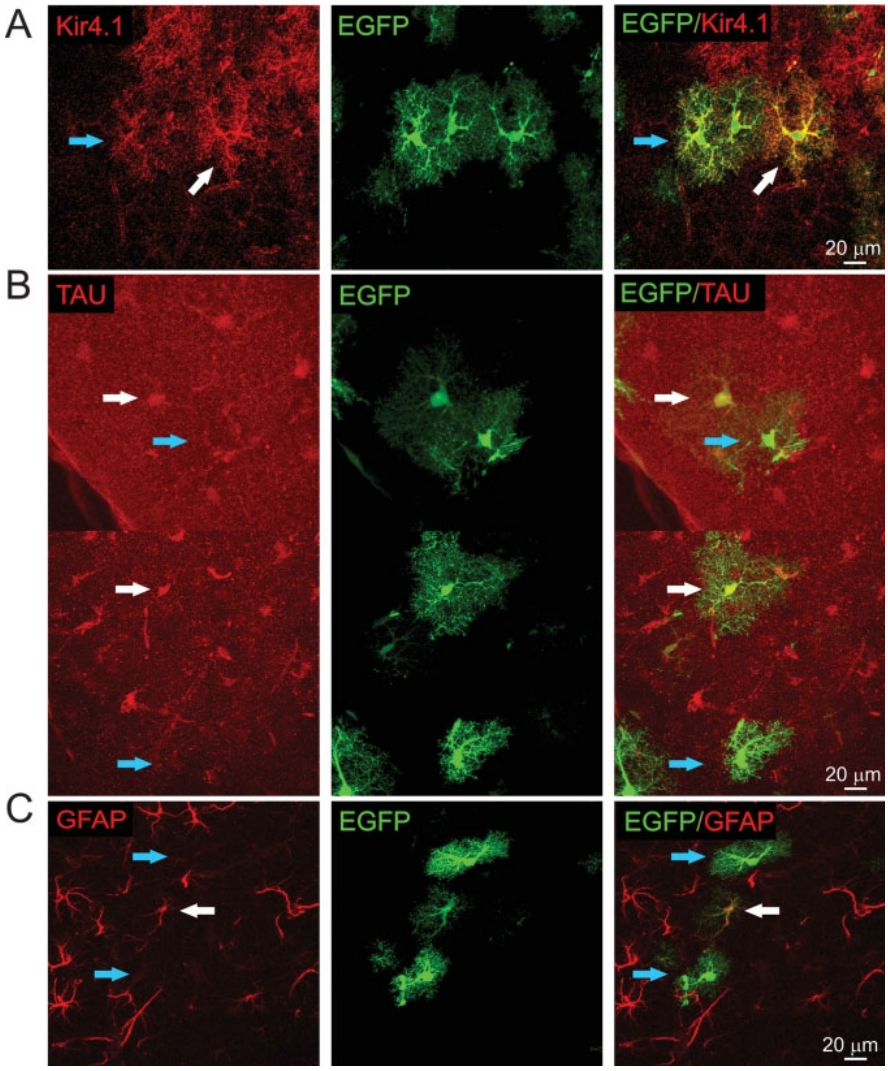

Figure 12: Immunohistochemical analysis of two distinct astrocyte populations in EGFP/GFAP mice. A: Both astrocytes strongly immunolabelled for Kir4.1 (white arrow) and astrocytes with lower Kir4.1 expression (blue arrow) are found in the brain of EGFP/GFAP mouse. B: Astrocytes treated with 1mM taurine solution show either strong (white arrow) or weaker taurine immunoreactivity (blue arrow). C: There are two different population regarding GFAP levels as well, some astrocytes do not have detectable levels of GFAP (blue arrows), while other astroglia strongly express this protein (white arrow). EGFP – enhanced green fluorescent protein; GFAP – glial fibrillary acid protein; Kir4.1 – inwardly rectifying K^+ protein; TAU – taurine. (Benesova et al. 2009)

Many methods were developed to study glial cell volume, its changes and cell morphology. They all have some advantages, but also limitations to various extent. There are methods good for detecting cell volume changes but give no or little information about morphology, such as measuring volume changes using intracellular fluorescent probe (Crowe

et al. 1995), confocal microscopy with transmitted light mode (Aitken et al. 1998) scanning ion conductance microscopy (Korchev et al. 2000) or monitoring differential pressure changes (Davis et al. 2004). Various methods were used to measure three dimensional (3D) structure of astrocytes. Electron microscopy has been widely used, displaying very fine astrocyte structure (Hama et al. 2004; Ogata and Kosaka 2002); however, processing of the cells in order to allow electron microscopy imaging may lead to significant deviations from the real native shape and cell dimensions (Chvatal, Anderova, and Kirchhoff 2007). 3D fluorescence imaging technique overcame some of the limitations of the electron microscopy and is used to study real-time effect of osmotic stress on astrocytes (Allansson et al. 1999), yet also has some disadvantages like possible phototoxicity of the fluorescent dye or relatively low resolution (Chvatal, Anderova, and Kirchhoff 2007). High temporal resolution is offered by phase-contrast video microscopy, but then this technique was designed for cell cultures (Boudreault and Grygorczyk 2004).

Astrocyte imaging *in vivo* and *in situ* was made a lot easier when transgenic mice with astroglia labelled by enhanced green fluorescent protein (EGFP) under the human GFAP promotor were generated, allowing to clearly distinguish astrocyte from neurons or other glial types (Nolte et al. 2001).

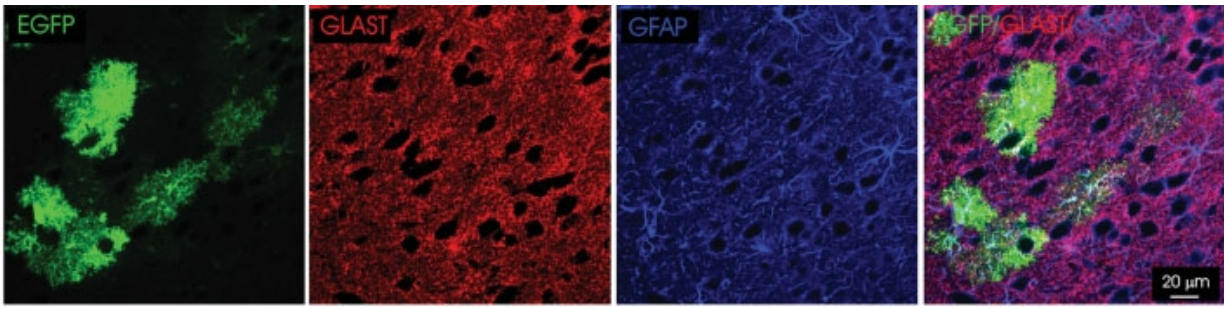

Figure 13: Astrocyte identification in EGFP/GFAP mice. Antibodies against astrocyte glutamate transporter GLAST and astrocyte marker GFAP were used in identification of EGFP positive cells in EGFP/GFAP mouse brain. EGFP – enhanced green fluorescent protein; GFAP – glial fibrillary acid protein; GLAST – glutamate aspartate transporter. (Benesova et al. 2009)

Imaging of cells in the living brain or spinal cord slices requires sufficient resolution and optical sectioning capability together with an excellent signal to noise ratio. Confocal microscopy and multiphoton microscopy fulfil these conditions and are widely used for 3D cell imaging (Benesova et al. 2009; Hirrlinger et al. 2008; Chvatal et al. 2007; Pannicke et al. 2010; Risher, Andrew, and Kirov 2009a). Confocal microscopy is a reliable tool in the imaging of moderately thick specimens. However, its penetration depth is limited when using

high numerical aperture lenses. Moreover, there is an extended photo-bleaching effect as the entire object is illuminated by the excitation light. In comparison, multiphoton microscopy has twofold penetration depth; nevertheless, resolution is not that high and the large light intensities cause bleaching in the focal plane (Pampaloni, Reynaud, and Stelzer 2007). Multiphoton microscopy is often employed in the imaging *in vivo* on living animals through cranial window, however, laser scanning confocal microscopy can be used as well, with similar results (Pérez-Alvarez, Araque, and Martín 2013).

Brain Aging

Aging is an inevitable process linked with overall decline in physiological functions, and with rising incidence of degenerative diseases and cancer (Rutten 2003). The brain aging process involves several macroscopic and microscopic structural changes that consequently result in functional changes, with major functional deficiency being cognitive impairment caused mainly by defects in neocortical and hippocampal circuitry. These changes are evolving without being necessarily induced by any specific disease (Salminen et al. 2011).

Macroscopic changes are evident by using non-invasive imaging techniques. Brain volume decreases with age in diffuse uniform manner in white matter and with some regional differences in the grey matter. The decrease is apparent particularly in individuals over the age of 70 years. The ventricular system and also the subarachnoid space enlarge in order to fill vacated space (Esiri 2007). Overall, the number of neurons is not significantly reduced (Esiri 2007; Salminen et al. 2011), although in some brain regions like neocortex or hippocampus, the loss of neurons is noticeable (Pakkenberg and Gundersen 1997; Simic et al. 1997). Additionally, there is a loss of myelinated fibres in white matter and shrinkage and dysmorphology of neurons (Pakkenberg and Gundersen 1997; Raz and Rodrigue 2006). Synapses are also affected; their numbers are distinctively decreased as a consequence of reduced dendritic and axonal arborisation. Moreover, the dendritic spines are diminished radically, in some regions the decrease with age is almost 50% (Esiri 2007; Jacobs, Driscoll, and Schall 1997; Raz and Rodrigue 2006; Salminen et al. 2011).

Aging is associated with increased levels of cellular stress (Salminen et al. 2011). Regarding great demand of neurons for oxidative metabolism when generating energy, it is especially the oxidative stress that contributes to aging process in the brain. Mitochondrial activity is inevitable for oxidative metabolism. This activity is coupled with generation of

oxygen free radicals that are very dangerous and may damage proteins, nucleic acids and also lipids. Mitochondria themselves may suffer oxidative damage and therefore, they become less productive in generating energy and even liable to generate more free radicals (Esiri 2007). Generally, DNA damage is either repaired or the cell with defective DNA undergoes apoptosis, however, this is often not the case in the aging brain. DNA repair mechanisms are failing and cells with accumulated impaired DNA are not eliminated (Rutten 2003). DNA damage leads to abnormal gene expression, either reduced or preserved but creating aberrant proteins that should be eliminated (Esiri 2007). Additionally, the mitochondria damage is associated with disruption of calcium homeostasis in neurons. Since the ability of mitochondria to store certain amounts of Ca^{2+} is impaired during aging, the intracellular space of neurons is exposed to elevated Ca^{2+} concentrations, especially during excitation. Such increase in intracellular Ca^{2+} levels may lead to activation of calcium-activated proteases with various potentially damaging effects. Presumably, these elevated Ca^{2+} levels are compatible with normal neuronal transmission, however, they make the brain very susceptible to damage by any stress (Esiri 2007).

Another typical aging indicator is accumulation of autophagic vacuoles containing pigments, such as lipofuscin or neuromelanin, originating from incompletely degraded proteins and lipids. These vacuoles may eventually occupy major part of the neuronal cell, interfering with its normal functions (Sulzer et al. 2008).

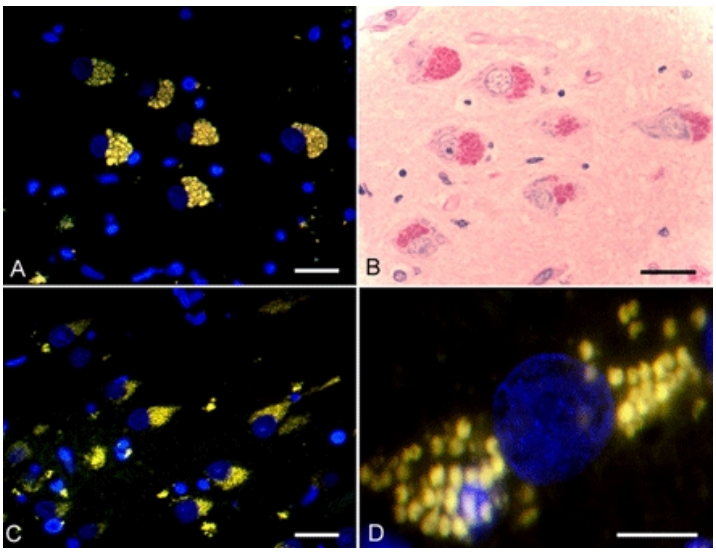

Figure 14: Lipofuscin in neurons of the aging human brain. Vacuoles filled with the autofluorescent pigment are shown in the cytoplasm of the neurons that are counterstained with 4',6-diamidino-2-phenylindole (DAPI; blue) under UV light (A,C,D) or stained red with the periodic acid-Schiff staining method (B). Scale bar: 30µm (A, B, C) and 10µm (D). (Gray and Woulfe 2005)

Expression of many genes changes during aging, some of them are downregulated while the expression of other genes is increased. In agreement with findings discussed above, downregulated genes are mainly those associated with synaptic transmission, mitochondrial function and Ca^{2+} homeostasis, while upregulated genes are usually linked with inflammation (Blalock et al. 2003). According to several gene expression profiles, the brain aging process provokes proinflammatory phenotype reflected by rising numbers of microglia and cytokine levels and also by the activation of the complement system (Salminen et al. 2011).

Aging of the glial cells

These above listed major changes, which take place in the aging brain, predominantly concern neurons. However, glial cells, such as astrocytes, microglia and oligodendrocytes, are equally affected by aging and alterations in their functions are not secondary to neuronal degeneration (Finch 2003). The current research turns the attention towards elucidating the role of glial cells in CNS aging as these cells provide numerous homeostatic functions that enable a proper neuronal functioning.

Microglia play a key role in the immune surveillance of the CNS, its development and plasticity. They are continuously surveying the microenvironment with their long motile processes, monitoring synapses and clearing apoptotic debris. Microglia represent the first and main form of active immune defence in the brain. Their morphology, cell surface antigens and secretory phenotype are transformed in response to homeostasis disturbances and such altered microglia are referred to as activated. They propagate the inflammatory signal by releasing pro-inflammatory cytokines (interleukin 1, interleukin 6, tumor necrosis factor α), followed by the release of secondary inflammatory mediators, such as prostaglandins and nitric oxides. The state of activated microglia is transient and after the inflammatory stimulus subsides, microglia returns to the surveillance mode (Heneka, Rodríguez, and Verkhratsky 2010; Norden and Godbout 2013; Ransohoff and Perry 2009). During aging, microglia undergo major morphology changes, such as deramification and fragmentation of the processes and cytoplasm (Streit et al. 2004).

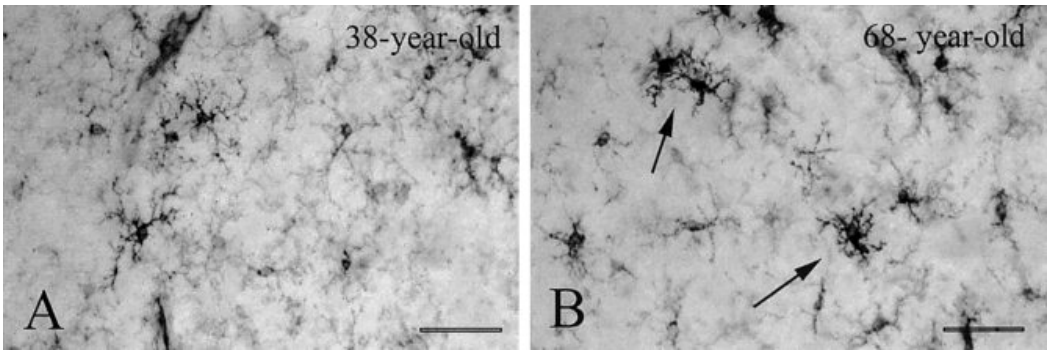

Figure 15: Adult and old microglia. Finely branched microglia found in the brain of 38-year-old (A) in comparison with dystrophic microglia (arrows) located in the brain of 68-year-old (B). Scale bar: 50μm. (Streit et al. 2004)

Same as for neurons, microglial mitochondria become increasingly damaged by oxidative stress and there is elevated intracellular accumulation of lipofuscin and some other substances (Brown 2009). Aged microglia exhibit lower levels of glutathione, which is responsible for the protection against reactive oxygen species (ROS), suggesting another functional impairment. In addition, internalization of amyloid β is significantly reduced with age (Njie et al. 2012). Secretory phenotype changes as well, microglia constitutively release larger amount of interleukin 6 (Il-6) and tumor necrosis factor α (TNFα) (Njie et al. 2012). Additionally, the expression of major histocompatibility complex class II molecules (MHC II) is higher and the regulatory systems, that are keeping microglia in their surveillance state, are impaired, therefore response to an immune challenge is amplified and more persistent (Norden and Godbout 2013).

Oligodendrocytes are responsible for creating and enwrapping myelin sheaths around axons and they produce mediators inducing clustering of the neuronal sodium channels and neuronal trophic factors (McTigue and Tripathi 2008). During aging, some oligodendrocytes degenerate but on account of their progenitors, which are still present in the brain, new cells are produced. When these two processes are balanced, oligodendrocyte numbers are stable; however, generally, one of them surpasses the other in the aging brain. Studies on old monkeys indicate that the number of oligodendrocytes increases with age (Peters and Sethares 2004); in the opposite, cell counts in the human brains revealed a decrease in their quantity (Pelvig et al. 2008). Myelin sheaths undergo age-related changes, such as the local splitting and the formation of blebs, when the sheath is ballooning. These alteration may lead to myelin degeneration. However, the formation of myelin continues also in the aging brain and the degeneration may be followed by the remyelination. Nonetheless, these new sheaths do

not reach the quality of the old ones and the conduction velocity along axons decreases, which might be one of the reasons of cognitive decline (Pannese 2013; Peters and Sethares 2004).

Astrocytes in the aging brain

According to the counting studies performed both on human and mouse brains, astrocyte numbers do not significantly diminish during aging (Fabricius, Jacobsen, and Pakkenberg 2013; Grosche et al. 2013; Pelvig et al. 2008). Employing levels of molecular markers give perplexing results. Beta-subunit of Ca^{2+} binding protein S100β shows an increase in astrocytes of the aging hippocampus, while GS levels show a decrease, affecting astrocyte role in neurotransmission (Rodríguez et al. 2014). Although many studies suggest an increase in GFAP levels, this phenomenon occurs predominantly in the hippocampus, while in most of the CNS regions rather a decrease in GFAP was detected (Cotrina and Nedergaard 2002; Lynch et al. 2010; Rodríguez et al. 2014; Salminen et al. 2011).

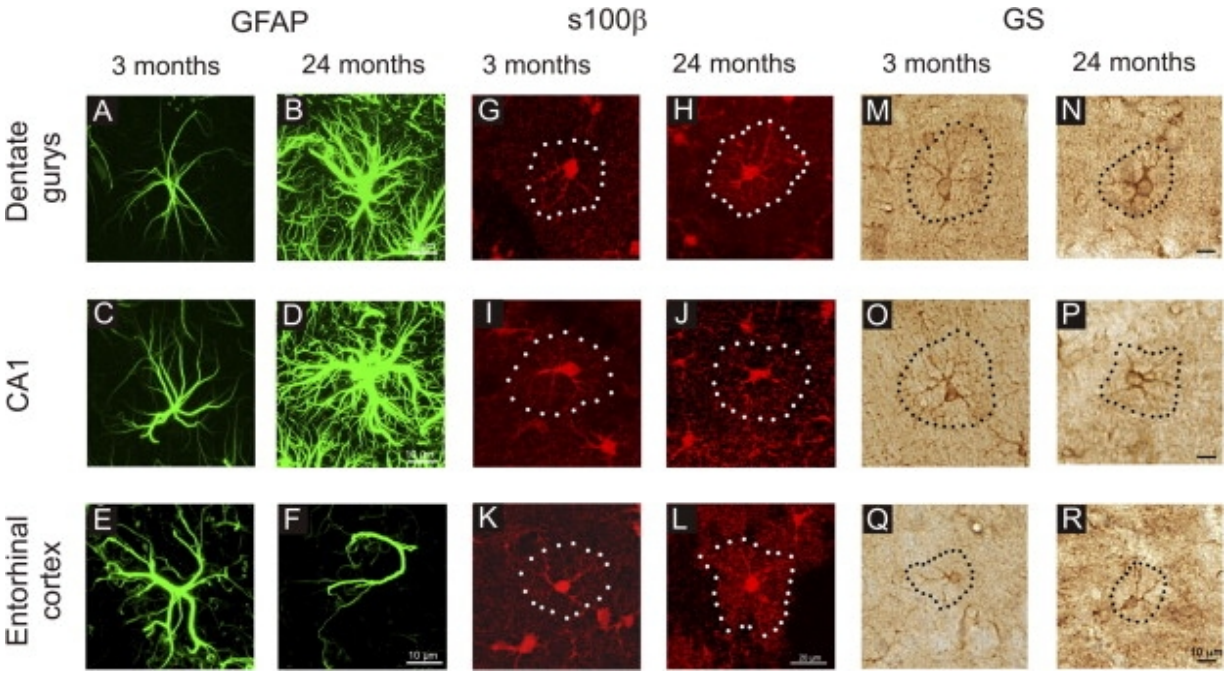

Figure 16: Age-dependent changes of the astrocyte molecular markers in different brain regions. Comparison between 3 month-old and 24 month-old mice astrocytes is shown in dentate gyrus, CA1 and enthorinal cortex. Both increase and decrease can be seen in GFAP (A-F), s100β (G-L) and GS levels (M-R). CA1 - cornu ammonis 1; GFAP – glial fibrillary acid protein; GS – glutamine synthetase. (Rodríguez-Arellano et al. 2015)

GFAP changes go hand in hand with changes in the overall cell volume, resulting either in cell atrophy or hypertrophy. Hypertrophy is associated with astrogliosis, which may be triggered by various brain insults, e.g. the neuroinflammation often attributed to aging

(Lynch et al. 2010; Rodríguez et al. 2014). On the other hand, there is astroglial atrophy, which may cause reduced neuronal connectivity as astrocytes retract their processes, loose contact with synapses and are unable to support neurons. This can be observed in the early stage of many neurodegenerative diseases (Heneka, Rodríguez, and Verkhratsky 2010; Rodríguez et al. 2014). Functional consequences of GFAP level changes are still unknown. Studies on astrocytes with either reduced GFAP levels or with completely absent GFAP suggest that lack of this protein results in enhanced long-term potentiation (LTP) and improved neuronal survival (McCall et al. 1996; Menet et al. 2000). Additionally, mice with highly enhanced expression of GFAP are dying few weeks after birth (Messing et al. 1998), implying that the excess accumulation of GFAP in astrocytes may be lethal.

The integrity and function of blood-brain barrier (BBB) is failing during aging and one of the reasons is growing population of senescent astrocytes (Bhat et al. 2012; Salminen et al. 2011; Zeevi et al. 2010). Astroglia in the aging brain present so called senescence-associated secretory phenotype (SASP) with typical elevated production of multiple inflammatory cytokines. The most significant is the increase in production of IL-6 (Bhat et al. 2012; Salminen et al. 2011), that together with other cytokines and prostaglandins increases the permeability of BBB, leaving the brain more susceptible to penetration of toxins and other ineligible substances (Abbott, Rönnbäck, and Hansson 2006). Additionally, BBB is affected by free radicals that are generated during aging, e.g. because of the iron excess accumulation in the perivascular astrocytes (Popescu et al. 2009).

Aging also affects the expression of astrocyte glutamate and purinergic receptors. As number of α-amino-3-hydroxy-5-methyl-4-isoxazolepropionic acid (AMPA) receptors is progressively decreasing with age, numbers of NMDA and P2X receptors are increasing at first, but then they start to decline at the old age, influencing glial synaptic currents (Lalo et al. 2011). Therefore, neurotransmitter induced Ca^{2+} signalling is likewise reduced (Rodríguez-Arellano et al. 2015). However, findings in cultured astrocytes show that old cells present Ca^{2+} waves of higher amplitude and faster oscillations than the young ones through stimulation of purinergic P2Y receptors, suggesting their expression might be increasing in aged brains (Watts and Lechleiter 2009).

As mentioned before, astrocytes usually create individual domains that are predominantly non-overlapping in adult mice. However, during aging, astrocyte cell volume is rising and their processes overlap much more. The reason for this swelling is still not clear.

Astrocytes may compensate for the decreasing functionality and capability to support neurons or the increasing oxidative stress, often associated with aging, might impair their volume regulatory mechanisms (Grosche et al. 2013).

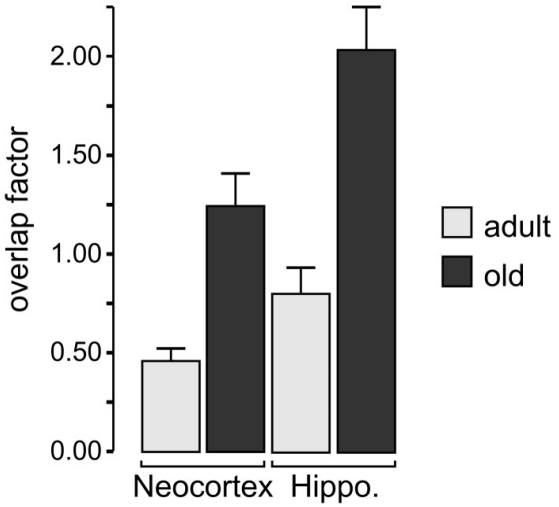

Figure 17: Astrocyte overlap factor in mouse neocortex and hippocampus. Overlap factor was calculated by multiplying the absolute number of astrocyte by the average astrocyte territorial volume and dividing the result by the volume of the studied brain tissue. The overlap factor more than doubled between adult (5 month-old) and old (21 months-old) mice. (Grosche et al. 2013)

Moreover, changes in GFAP levels influence cell volume regulation, as some of the cell-volume sensors are cytoskeleton-linked stretch-activated plasma membrane channels (Pekny and Nilsson 2005). Mice lacking GFAP and vimentin, crucial components of astrocyte intermediate filaments, present much lower efflux of taurine, important in RVD (Ding et al. 1998). Furthermore, astrocytes from transgenic mice lacking GFAP ($GFAP^{-/-}$) exposed to osmotic stress exhibit smaller K^+ concentration in the vicinity of the cells compared to wild type astroglia; suggesting restricted swelling of $GFAP^{-/-}$ astrocytes (Anderova et al. 2001). AQP4, another very important effector in cell volume regulation, is affected by age as well. Its perivascular polarization is lost in the aged brain and the paravascular expression is absent, too. Thus, the clearance through paravascular pathways is impaired and it may result in accumulation of interstitial solutes like amyloid β (Kress et al. 2014). Loss of AQP4 specific localization influences also the volume regulation, such astrocytes present smaller volume changes and altered regulatory mechanisms in response to severe hypo- or hyperosmotic stress (Anderova et al. 2014).

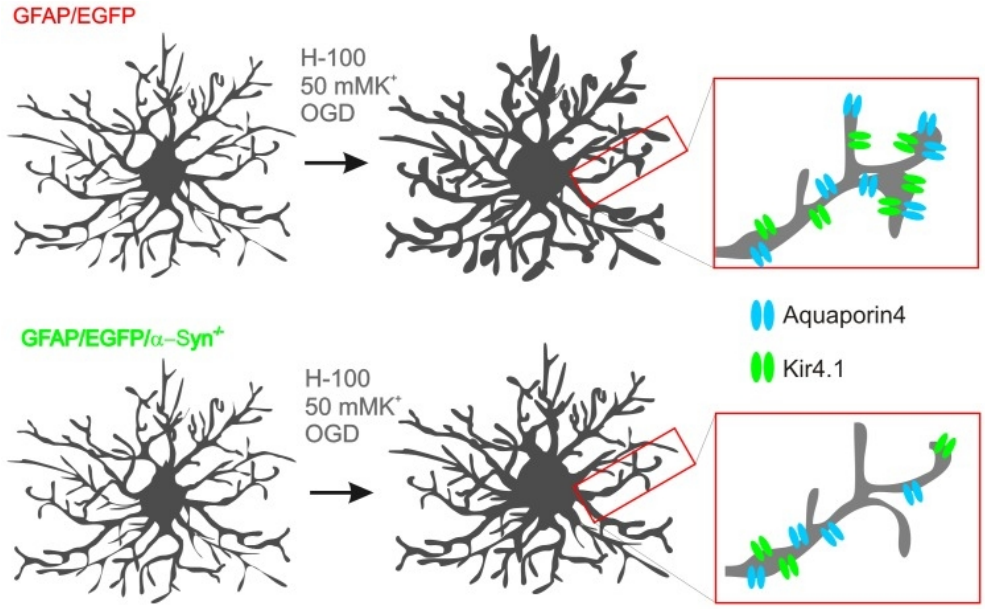

Figure 18: Differences in astrocyte swelling in α-syntrophin lacking mice. Schematic comparison between GFAP/EGFP mice and mice expressing EGFP under human GFAP promotor and additionally lacking α-syntrophin (GFAP/EGFP/α-Syn$^{-/-}$), protein important for site-specific anchoring of aquaporin4 (AQP4) and for co-localization of AQP4 and Kir4.1. In response to severe hypoosmotic stress, increased extracellular K^+ concentration or oxygen glucose deprivation, swelling of GFAP/EGFP/α-Syn$^{-/-}$ astrocyte processes is smaller than the swelling of astrocyte process in EGFP/GFAP brain. As the scheme suggests, smaller swelling occurs because of lower expression of aquaporin4 and Kir4.1 at the endfeet. 50mMK^+ - solution with elevated K^+ concentration (50mM); α-Syn – α-syntrophin; EGFP – enhanced green fluorescent protein; GFAP – glial fibrillary acid protein; H-100 – hypoosmotic stress solution (205mOsm/kg), Kir4.1 - inwardly rectifying K^+ channel; OGD – oxygen glucose deprivation. (Anderova et al. 2014)

In spite of the fact that astroglia become activated early in the aging process without concurrent pathology (Finch 2003), evidence on the age affected expression pattern of many ion channels and co-transporters is still missing and only a small number of *in vivo* studies is focused on the process of normal physiological aging and the role of astroglia. Moreover, many of the findings discussed above are contradictive, therefore a lot of work has yet to be done before a systematic concept on astroglial aging would be established.

Aims of the study

I. To study time-dependent volume changes of astrocytes induced by elevated K^+ concentration during aging.

II. To study time-dependent volume changes of astrocytes induced by hypoosmotic stress during aging.

III. To determine whether there are any sex-dependent changes.

Materials and Methods

Animals

Female and male EGFP/GFAP mice (Nolte et al. 2001) at the age of 3, 9, 12 and 18 months were used in the experiment. All animals were kept at the Institute of Experimental Medicine AS CR in an air conditioned animal facility at a temperature of 20-25°C under 12-hour light/dark cycle with a free access to food and water. All procedures involving the use of laboratory animals were performed in accordance with the European Communities Council Directive 24 November 1986 (86/609/EEC) and animal care guidelines approved by the Institute of Experimental Medicine ASCR Animal Care Committee.

Visualization of astrocytes from EGFP/GFAP mice is possible thanks to enhanced expression of green fluorescent protein (EGFP), which is under the control of the human GFAP promoter. Confocal microscopy allows direct imaging of even the fine astrocyte processes and direct measuring of volume changes in single astrocyte can be done via three-dimensional (3D) confocal morphometry.

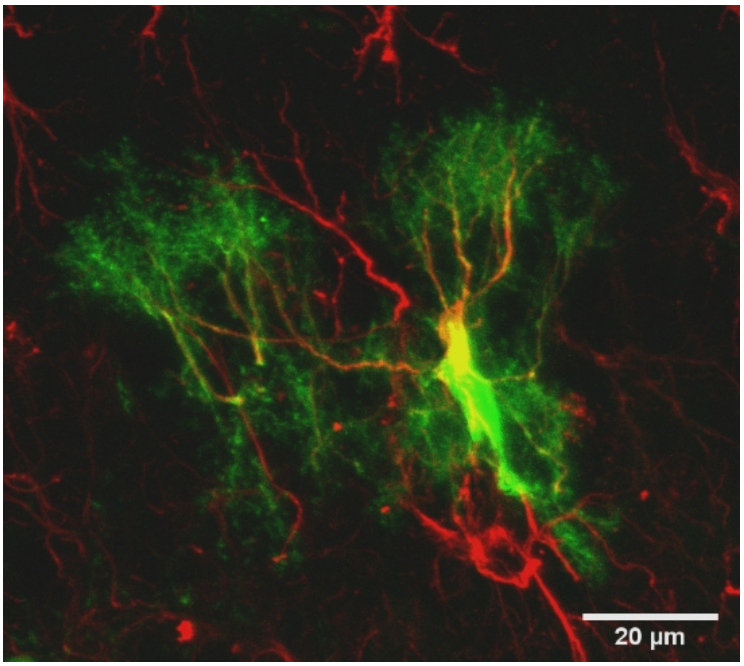

Figure 19: Co-localization of EGFP (green) and immunohistochemically labelled GFAP (red) in hippocampal astrocyte of EGFP/GFAP mouse. EGFP – enhanced green fluorescent protein; GFAP glial fibrillary acid protein.

Preparation of acute brain slices

EGFP/GFAP mice were anesthetized by intraperitoneal injection of lethal dose (100 mg/kg) of 1% sodium-pentobarbital (PTB) diluted in 0.9% physiological saline (Sigma-Aldrich, St. Louis, MO, USA). An incision through the skin was made along the thoracic midline from the xiphoid process to the clavicle and the thoracic cavity was open by cutting the diaphragm from one lateral aspect to the other while avoiding cutting any visceral organs. Both lateral aspects of the rib cage were cut in rostral direction. After exposing the thoracic organs, the right atrium of the heart was cut and a needle attached to a perfusion syringe was inserted into the left ventricle. Transcardial perfusion with isolation solution (composition listed in Table 1) was performed in order to cool down the brain, clear the blood and replace the Na^+ to protect the brain tissue. The mouse was rapidly decapitated and the severed head was transferred into silicon-coated Petri dish filled with ice-cold isolation solution. The scalp was cut along the midline to expose the scull, which was then carefully removed using tweezers and microdissecting scissors. The olfactory bulb and cerebellum were cut off with scalpel and the rest of the brain was removed from the braincase and glued to the specimen disc with its ventral part leaning at a solid agar cube, using Vetbond tissue adhesive (3M, Saint Paul, MN, USA). The disc was then transferred into the vibration microtome chamber (Microm HM 650V, Thermo Fisher Scientific, Waldorf, Germany) containing cold isolation solution (~4°C) bubbled with 95% O2 and 5% CO2 (carbogen; Siad, Branany, Czech republic) and 300 μm thick transverse slices were cut with razor blade. The slices were then incubated for 40 minutes at 34°C in the isolation solution. After the incubation period, the slices were kept at room temperature in artificial cerebrospinal solution (aCSF solution, Table 1). All solutions were equilibrated with 95% O_2/5% CO_2 to final pH of 7.4. Osmolality was measured using a vapor pressure osmometer (Vapro 5520, Wescor, Logan, UT), pH value was determined using pH meter MiniLab IQ125 (IQ Scientific Instruments, San Diego, USA).

During the actual experiment, slices were cut in half (to obtain separate left and right hemisphere) and placed carefully into the recording chamber mounted on the stage of a confocal microscope. The slices were held down with a U-shaped platinum wire with a grid of nylon threads. The recording chamber was continuously perfused with recording solutions via a peristaltic pump PCD 31.2 (Peristaltická čerpadla a dávkovače Ing. Jindřich Kouřil, Kyjov, Czech Republic) at a rate of ~5 ml/min. Teflon tubing was used to prevent changes in gas content during perfusion. Peristaltic pump has two separate circuits for influx and efflux, therefore perfusion solution can be changed by a simple transfer of the influx tube. The

change of solutions in the recording chamber can be observed approximately after 2 minutes. All measurements were performed at 22-24°C.

Solutions

The compositions of brain isolation solution, artificial cerebrospinal fluid (aCSF), solution with elevated potassium concentration ($aCSF_{K+}$) and hypotonic solution ($aCSF_{H-100}$) are listed in Table 1. Each solution was equilibrated with 95% O_2 and 5% CO_2 and pH was 7.4.

Table 1: Composition of the solutions. aCSF – artificial cerebrospinal fluid; $aCSF_{H-100}$ - hypotonic solution; $aCSF_{K+}$ - solution with elevated potassium concentration; NMDG – N-methyl-D-glucamine.

	Concentration [mM]			
	aCSF	***Isolation solution***	***$aCSF_{K+}$***	***$aCSF_{H-100}$***
2M NaCl	122	-	75	-
NMDG	-	110	-	-
1M KCl	3	2.5	50	2
0.5M $NaHCO_3$	28	24.5	28	26
0.1M Na_2HPO_4	1.25	1.25	1.25	1.25
Glucose	10	20	10	10
1M $CaCl_2$	1.5	0.5	1.5	1
1M $MgCl_2$	1.3	7	1.3	1
	Osmolarity [mOsmol/kg]			
	300±10	300±10	300±10	200±10

Three-dimensional Confocal Morphometry

To determine astrocyte volume changes, 3D confocal morphometry was used (Benesova et al. 2009; Chvatal, Anderova, and Kirchhoff 2007; Chvatal et al. 2007). A confocal microscope (Leica TCS SP, Solms, Germany) equipped with Ar/HeNe laser and a Leica x40 (0.8) HCX APO water-immersion objective was employed in the experiments. Ar laser was set at 488nm for the excitation of EGFP, and emitted light was recorded over the range of 510 – 552 nm with a TD488/543/633 filter. Laser intensity was always only 30% in order to minimalize photobleaching. Pinhole was set to 2.5 Airy. The range of gain varied from 700 to 800 (artificial units) and the offset was around 51-52%.

Three-dimensional image of an individual astrocyte *in situ* was generated from the stack of 75-85 consecutive two-dimensional images, made by sectioning the astrocyte along

the vertical axis into a set of parallel uniformly spaced (1-1.5 μm) two-dimensional (2D) confocal planes. Each image had a resolution of 1024x1024 pixels. Leica Confocal Software (Leica, Solms, Germany) was employed for collecting and saving the data.

Image processing and the morphometric measurements were performed using the CellAnalyst software, which was developed in the Department of Cellular Neurophysiology, Institute of Experimental Medicine, Prague, Czech Republic and which enables filtering of the images, including removing of the background noise, thresholding the image and morphometric calculations (Chvatal et al. 2007).

An area of the image was considered to be part of the cell only when the pixel values were above the threshold of 30-50 of the gray scale (0-255). Volume of the astrocyte was calculated by summing up the areas selected by the thresholding of all images in a stack and multiplying this sum by the distance between two neighboring sections, as shows the following equation:

$$V = T \cdot \sum_{i=1}^{n} U_i$$

where V is the cell volume, T is the distance between sections, U is the unit area and n is the number of sections.

Volume changes were studied in astrocytes located in the *Cornu Ammonis* 1 (CA1) region of the hippocampus. The total acquisition time for a stack of 75-85 images was approximately 240 sec.

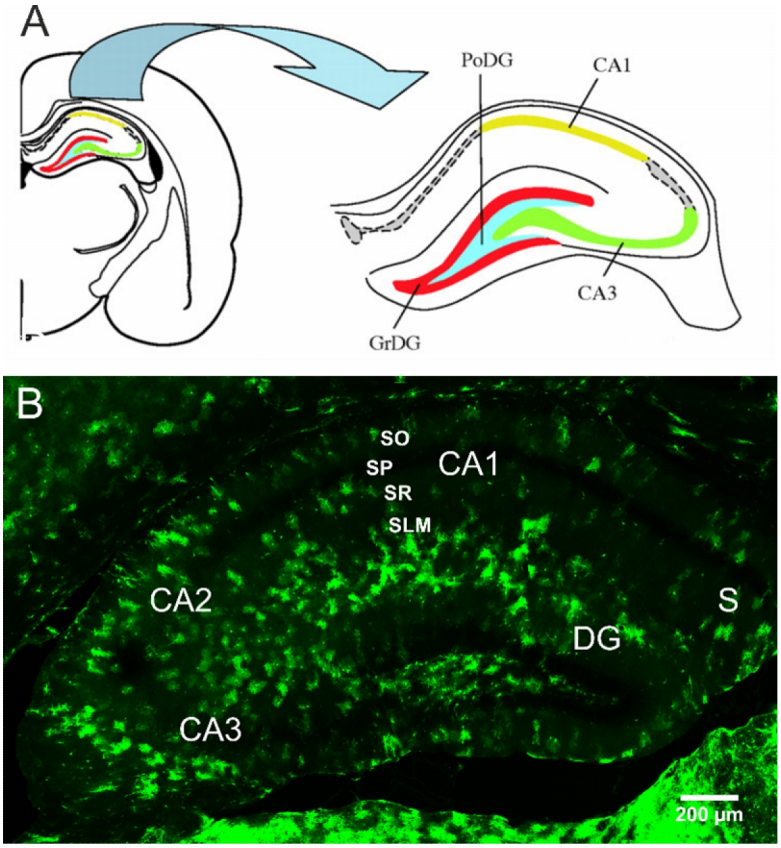

Figure 20: ***Cornu Ammonis 1*** **in a mouse hippocampus.** All the volume changes recorded in this experiment were studied in CA1 region. Schematic layout (A) shows different regions of mouse hippocampus with CA1 region marked yellow (Burger et al. 2010). Different layers of CA1 can be seen in EGFP/GFAP mouse hippocampus (B). CA1 – cornu ammonis 1; CA 2 – cornu ammonis 2; CA3 – cornu ammonis 3, DG – dentate gyrus; GrDG – granular layer of the dentate gyrus; PoDG – polymorph layer of the dentate gyrus; S – subiculum; SLM – stratum lacunosum-moleculare; SO – stratum oriens; SP – stratum pyramidale; SR – stratum radiatum

Exposure to the light of excitatory laser during the confocal scanning decreased the intensity of the EGFP fluorescence. To avoid any miscalculation caused by this photobleaching, three consecutive control measurements were made for each individual astrocyte using aCSF for perfusion. These data were not only used to calculate astrocyte volume prior to pathological stimulus, but also to form an algorithm to compensate for the signal decrease. Three measurements in aCSF were followed either by the application of $aCSF_{H\text{-}100}$ or $aCSF_{K+}$, for 20minutes and followed by the application of aCSF (further termed wash-out).

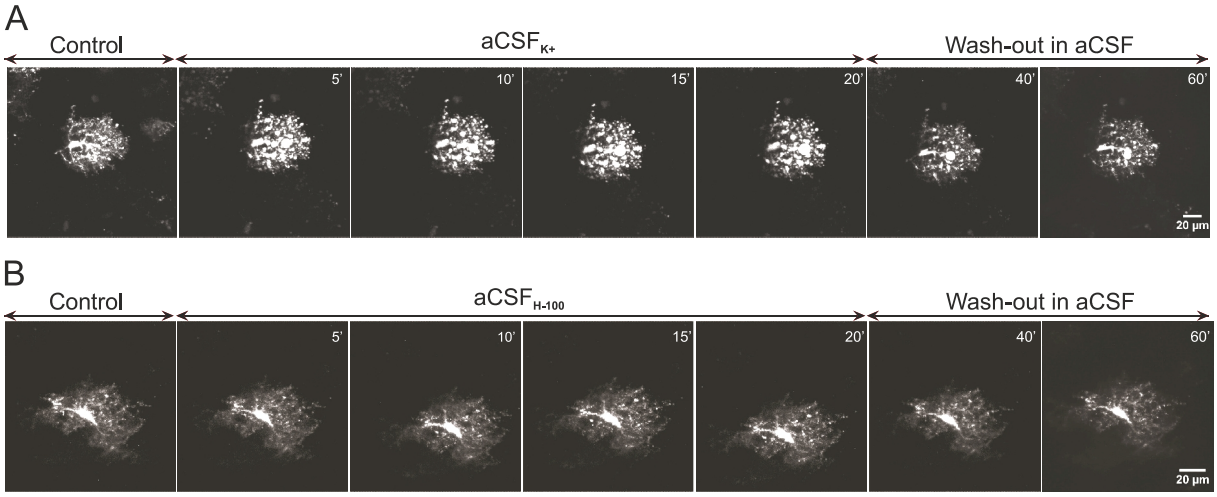

Figure 21: Astrocyte volume changes during osmotic stress. Superimposed images of hippocampal astrocytes from EGFP/GFAP mice were recorded at different times during measurement. Control image was taken during the application of aCSF, followed by the application of either $aCSF_{K+}$ (A) or $aCSF_{H-100}$ (B) for 20 minutes. Astrocyte volume was quantified every 5 minutes. Last two stacks of images were recorded at the interval of 20 minutes during 40-minute wash-out, again in aCSF. aCSF – artificial cerebrospinal fluid; $aCSF_{K+}$ - solution with elevated K^+ concentration; $aCSF_{H-100}$ - hypotonic solution.

Relative changes of astrocyte volume are given as percentages of control values.

Immunohistochemistry

EGFP/GFAP mice were anesthetized by intraperitoneal injection of 1% PTB and perfused transcardially with 20ml of physiological solution with heparin (100 ml/0.65 ml) and then with 20ml of 4% paraformaldehyde (PFA). The brain was dissected from the skull (same protocol as above) and put in 4% PFA to be fixed overnight. Next, it was dehydrated through sucrose gradient (10%, 20% and 30% sucrose), frozen and cut into 30µm slices using cryotome Hyrex C50 (Zeiss, Oberkochen, Germany). Slices were incubated for 2 hours in blocking buffer (10 mM phosphate-buffered saline containing 0.5% Triton; Sigma and 5% Chemiblocker; Millipore, Billerica, MA, USA) to permeabilize cell membranes and prevent non-specific staining. Afterwards, they were incubated with primary antibody rabbit anti-NG2 (1:400, Millipore, Billerica, MA, USA) or rabbit anti-GFAP (1:800, Sigma-Aldrich, St. Luis, MO, USA) at 4°C overnight and rinsed with phosphate-buffered saline (PBS; 1x15min, 2x10min). The secondary antibody goat anti-rabbit IgG conjugated with AlexaFluor 594 (1:200; Life Technologies, Carlsbad, CA, USA), was applied for 2 hours at 4°C. All antibodies were diluted in blocking buffer. Excessive antibodies were washed away with PBS. To visualize the cell nuclei, slices were mounted on microscope slides using Vectashield

mounting medium with 4', 6-diamidino-2-phenylindol (DAPI; Vector Laboratories, Burlingame, MI, USA).

Confocal Microscopy

A confocal microscope equipped with Ar laser and 60x water-immersion objective (Olympus FV1200MPE, Shinjuku, Japan) was employed to carry out immunohistochemical analyses. The gain and offset were adjusted to minimize saturated pixels but still allow the detection of weakly stained processes, for each stack of image separately.

Data Analysis

Data are presented as means ± standard error of the mean and the statistical significance was assessed by unpaired t test using GraphPad InStat software (GraphPad Software, La Jolla, CA, USA). P values under 0.05 were considered statistically significant (* $P < 0.05$; ** $P < 0.01$, *** $P < 0.001$). Graphs were created using GraphPad Prism software (GraphPad Software, La Jolla, CA, USA).

Results

Astrocyte volume changes induced by elevated K+ concentration

Identification of astrocytes in acute brain slices

Acute mouse brain slices were prepared as described in Materials and Methods. Using EGFP/GFAP mice allows direct imaging of astrocytes, which express enhanced green fluorescent protein (EGFP). For the experiment, cells were chosen from both the stratum radiatum and stratum oriens in the CA1 region of the hippocampus. Astrocytes were not the only cells expressing EGFP in this region (Matthias et al. 2003), also a certain subpopulation of chondroitin sulphate proteoglycan expressing cells (further termed NG2 glia) expressed EGFP. However, astrocytes were clearly distinguishable based on their morphology. Their numerous processes radiating from the soma to all directions created branched nets and their fluorescence was very bright. In contrast, NG2 glia are characterized by short thin processes and dim fluorescence (Figure 22).

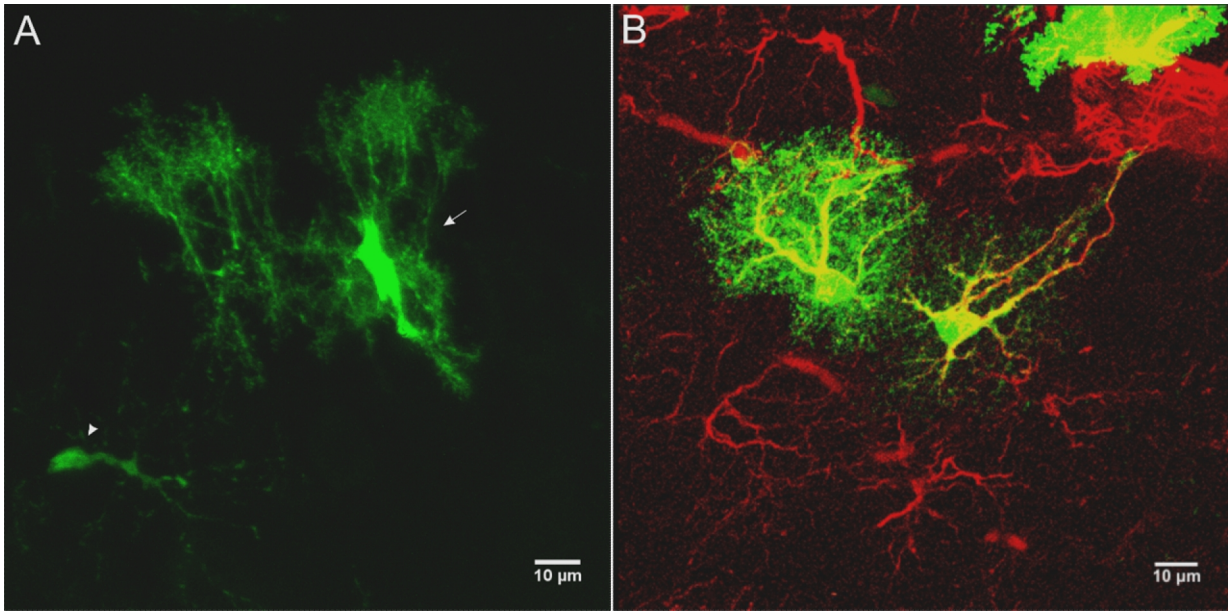

Figure 22: Hippocampal astrocyte and NG2 glia expressing EGFP. A: The larger and brighter cell is typical astrocyte with highly ramified processes (arrow). At the left bottom is NG2 glia, that is not as bright and its processes are thinner and less branched (arrowhead). **B:** Immunohistochemical identification of EGFP astrocytes using antibody against GFAP (red). EGFP – enhanced green fluorescent protein; GFAP – glial fibrillary acidic protein; NG2 – chondroitin sulphate proteoglycan NG2.

Time-dependent astrocyte volume changes induced by high extracellular concentration of K+

In order to determine how aging influences astrocyte cell volume regulation, acute brain slices from 3-months-old (3M), 9-months-old (9M), 12-months-old (12M) and 18-months-old (18M) EGFP/GFAP mice were prepared and put into the perfusion chamber in which they were exposed to extracellular K^+ concentration of 50mM. Such a high concentration of K^+ is typical for ischemic injury, reaching 50-70 mM K^+ (Siemkowicz and Hansen 1981; Zoremba et al. 2008). Astrocyte volume changes were recorded using upright confocal microscope. Firstly, aCSF was applied in order to record the original volume of the cell. Perfusion then continued with 20-minute application of $aCSF_{K+}$ followed by the wash-out with aCSF for 40 minutes. Cell volume was recorded each five minutes during $aCSF_{K+}$ application and each 20 minutes during wash-out (Figure 23).

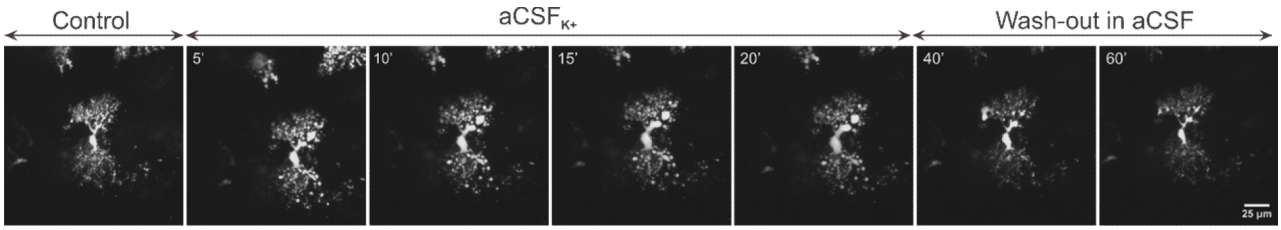

Figure 23: Astrocyte volume changes induced by high extracellular K^+ concentration. Superimposed images of astrocyte display its original volume (Control) and volume changes during $aCSF_{K+}$ application recorded every 5 minutes. Last two images show astrocyte volume after 20 and 40 minutes of the wash-out with aCSF. aCSF – artificial cerebrospinal fluid; $aCSF_{K+}$ - solution with elevated K^+ concentration.

In all age groups, marked swelling of astrocytes was obvious after the first five minutes of the $aCSF_{K+}$ application, when the cell volume rose steeply (Figure 24). After this increase, it remained more or less steady for the duration of $aCSF_{K+}$ application. At the beginning of the wash-out, astrocyte volume sharply returned back to the values around 100% and remained there also after 40 minute of the aCSF application. By comparing different age groups, it is evident that 3M and 12M astrocytes display higher rate of swelling than 9M and 18M. Significant differences between the volumes of 3M and 9M astrocytes were found during the entire application of $aCSF_{K+}$ and between the volumes of 9M and 12M astrocytes at 5^{th} and 10^{th} minute of the $aCSF_{K+}$ application.

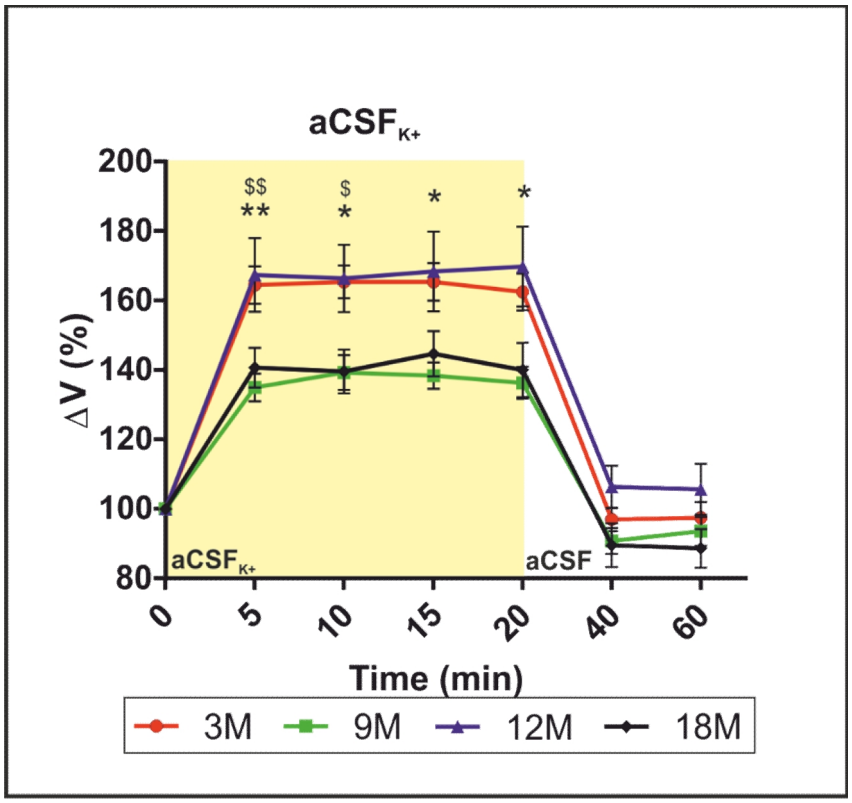

Figure 24: Volume changes of astrocytes induced by elevated K^+ concentration. Time-dependent volume changes of hippocampal astrocytes from EGFP/GFAP mice of different ages were recorded during 20-minute application of $aCSF_{K+}$ followed by 40-minute wash-out with aCSF. Data are given as percentage change ± SEM and the original volume is always represented as 100%. Asterisks indicate significant (*, $p<0.05$) and very significant (**, $p<0.01$) differences between the volumes of 3M and 9M astrocytes. Paragraphs indicate significant ($, $p<0.05$) and very significant ($$, $p<0.01$) differences between 9M and 12M cell volumes. 3M – 3-month-old mice; 9M – 9-month-old mice; 12M – 12-month-old mice; 18M – 18-month-old-mice; aCSF – artificial cerebrospinal fluid; $aCSF_{K+}$ – solution with elevated K^+ concentration; SEM – standard error of the mean.

Astrocyte volume changes in female and male EGFP/GFAP mice

The data from female and male EGFP/GFAP mice were evaluated separately to see whether there are sex-dependent differences between astrocyte responses to 50mM K^+. The trend in the female group (Figure 25A) was very similar to the overall trend seen above (Figure 24). Even the higher rate of swelling of 3M and 12M astrocytes when compared to 9M and 18M astrocytes was conserved. Significant differences between the age groups were found after 5 minutes of $aCSF_{K+}$ application between the volumes of female 9M and 12M astrocytes and during the wash-out, when 9M and 12M astrocytes differ at 20th minute and 12M and 18M cells at both points of aCSF application. In opposite, no significant difference between the four age groups was found in male astrocytes and the swelling rates of each age

group during the $aCSF_{K+}$ application were not as easily distinguishable as in the female astrocytes (Figure 25B). When looking at the data, it seems that during $aCSF_{K+}$ application, male 9M and 18M astrocytes tended to swell more than those of females, however this difference was not significant. Statistically significant differences between males and females were found only in 9M and 18M mice (Figure 25C and D). The volume decrease of 9M female astrocytes after first 20 minutes of aCSF application was significantly greater than the decrease in 9M male astrocytes and similar situation is seen in 18M mice, only after 40 minutes of aCSF wash-out.

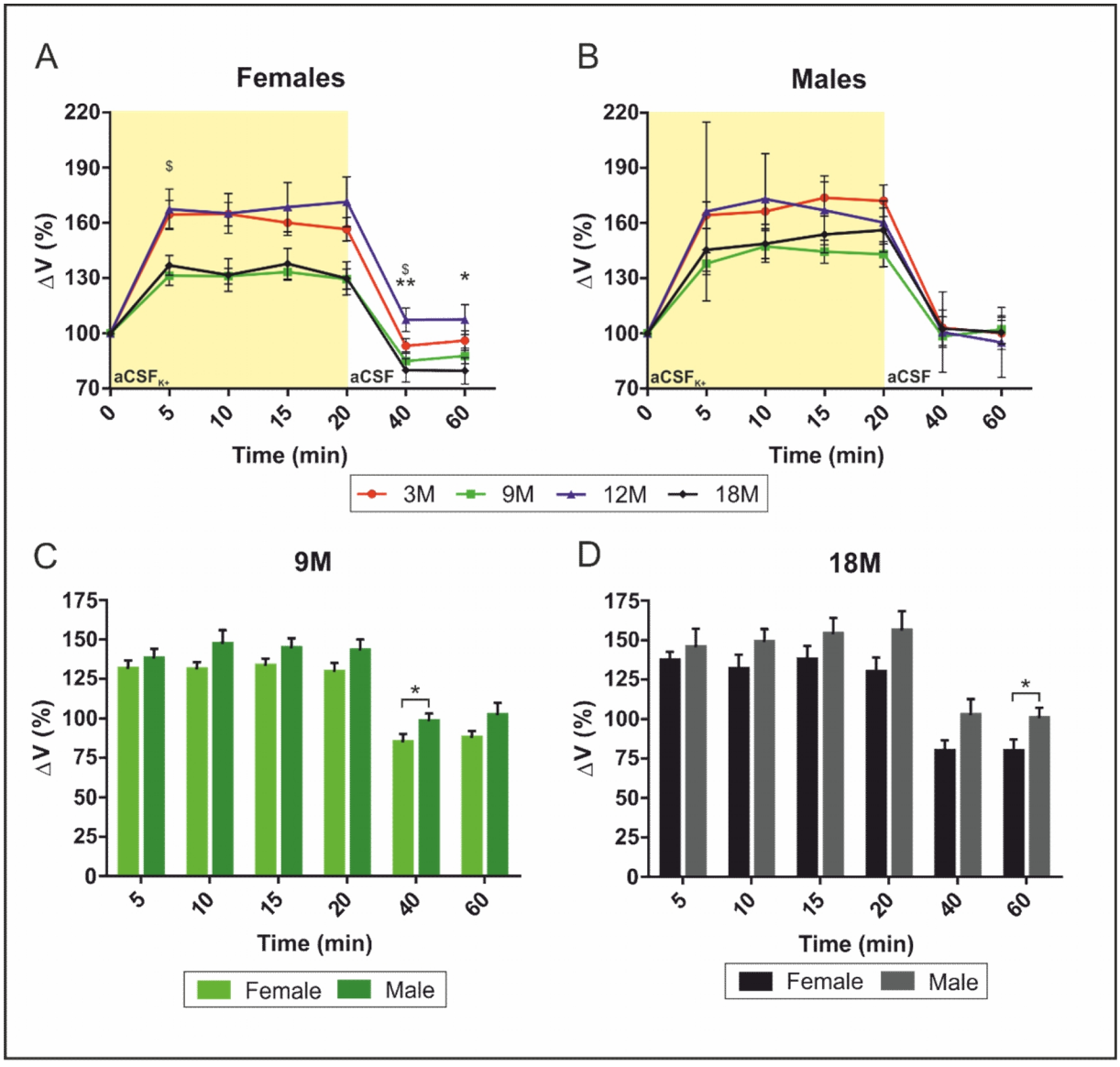

Figure 25: Astrocyte volume changes induced by elevated K^+ concentration in different sexes. **A+B**: Astrocyte volume was recorded during the application of $aCSF_{K+}$, followed by the application of aCSF and the data were evaluated as percentage changes ± SEM for female (A) and male (B) group separately. The original volume is expressed as 100% in both groups for all ages. Asterisks indicate significant (*, $p<0.05$) and

very significant (**, $p<0.01$) differences between the volumes of female 12M and 18M astrocytes and paragraphs indicate significant ($, $p<0.05$) differences between female 9M and 12M astrocyte volumes. **C+D:** Volume changes of astrocytes from 9- (C) and 18-month-old (D) female and male EGFP/GFAP mice, recorded during the 20-minute application of $aCSF_{K+}$ and the 40-minute wash-out with aCSF, are expressed as percentage changes + SEM. Asterisks show the only two significant (*, $p<0.05$) differences found between male and female mice of all age groups. 3M – 3-month-old mice; 9M – 9-month-old mice; 12M – 12-month-old mice; 18M – 18-month-old-mice; aCSF – artificial cerebrospinal fluid; $aCSF_{K+}$ – solution with elevated K^+ concentration; SEM – standard error of the mean.

Astrocyte volume changes induced by hypoosmotic stress

As described above, acute brain slices from EGFP/GFAP mice were perfused with different solutions simulating various extracellular conditions in order to characterize volume changes in aging. Besides $aCSF_{K+}$, $aCSF_{H-100}$ was used as the insult solution, making the astrocyte swell because of the hypoosmotic extracellular environment. As seen in Figure 26, the application scheme for $aCSF_{H-100}$ was the same as for $aCSF_{K+}$.

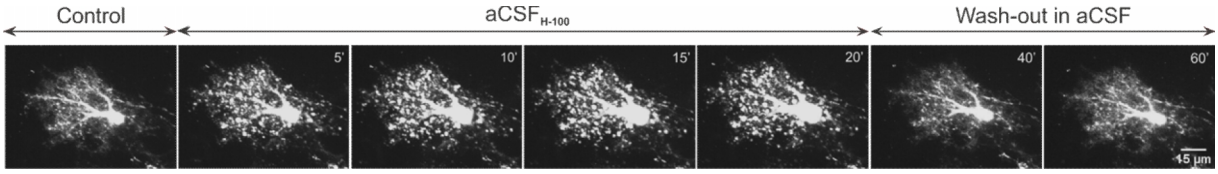

Figure 26: Astrocyte volume changes induced by hypoosmotic stress. Superimposed images of an astrocyte represent the volume changes during the 20-minute $aCSF_{H-100}$ application and following 40-minute wash-out with aCSF. Control image shows the original volume of the astrocyte at the beginning of measurement. aCSF – artificial cerebrospinal fluid; $aCSF_{H-100}$ – hypoosmotic solution.

Figure 27 depicts astrocyte swelling that occurred during the $aCSF_{H-100}$ application in all age groups. After first five minutes, the astrocyte volume increased steeply and the cells remained swollen until the start of the wash-out. After 20 minutes of aCSF application, cell volume returned to the values around 100% but then rose again in case of all age groups but 18M. This final volume increase was most apparent in 3M astrocytes. Significant differences between age groups were found at both points of wash-out. The volumes of 3M and 9M cells differ significantly after 20 minutes of aCSF application, whereas at 40^{th} minute, the extent of 3M astrocyte swelling was significantly higher when compared to all the other age groups.

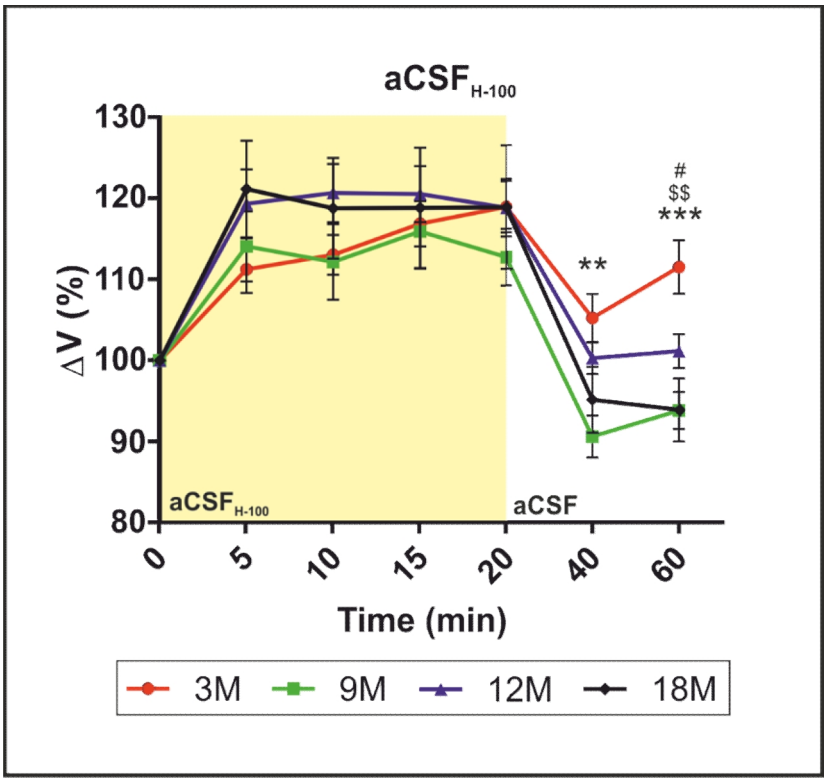

Figure 27: Volume changes of astrocytes during hypotonic stress. Time-dependent volume changes of hippocampal astrocytes from EGFP/GFAP mice of different age were measured during 20-minute application of $aCSF_{H-100}$ followed by 40-minute application of aCSF. The data are given as percentage change ± SEM and the original volume of astrocytes is always expressed as 100%. Asterisks indicate very significant (**, $p<0.01$) and extremely significant (***, $p<0.001$) differences between the volumes of 3M and 9M astrocytes. Paragraphs indicate very significant ($$, $p<0.01$) difference between the volumes of 3M and 18M astrocytes and the hashtag indicates significant (#, $p<0.05$) difference between 3M and 12M astrocyte volumes. 3M – 3-month-old mice; 9M – 9-month-old mice; 12M – 12-month-old mice; 18M – 18-month-old-mice; aCSF – artificial cerebrospinal fluid; $aCSF_{H-100}$ – hypotonic solution; SEM – standard error of the mean.

Hypoosmotic stress-induced astrocyte volume changes in female and male mice

Sex-dependent differences between astrocyte volume responses to hypoosmotic stress were investigated. As seen at Figure 28, both female and male astrocytes exhibited swelling during application of $aCSF_{H-100}$ and their volume decreased during first 20 minutes of wash-out. Then, the cell volume increased again after 40 minutes of aCSF application in almost all age groups, only in 18M female and 12M and 18M male astrocytes it further decreased. Significant difference between the four age groups was found only at the final point of wash-out. In female mice, there was statistically significant difference between the volumes of 3M and 18M astrocytes, whereas in male group 3M and 9M cells differed significantly. Even though the rate of swelling of 12M male astrocytes seemed to be a lot higher than the swelling rate of 12M female cells, this difference was not statistically significant. In fact, the only

significant difference between females and males was found at the age of 3M. After first 5 minutes of $aCSF_{H\text{-}100}$ application, 3M female astrocytes exhibited significantly greater volume increase than 3M male astrocytes. Moreover, 3M male astrocyte volume continually increased during $aCSF_{H\text{-}100}$ application, while in all other age groups, both male and female, the cell volume rose swiftly after first five minutes but then remained more or less stable till the start of wash-out.

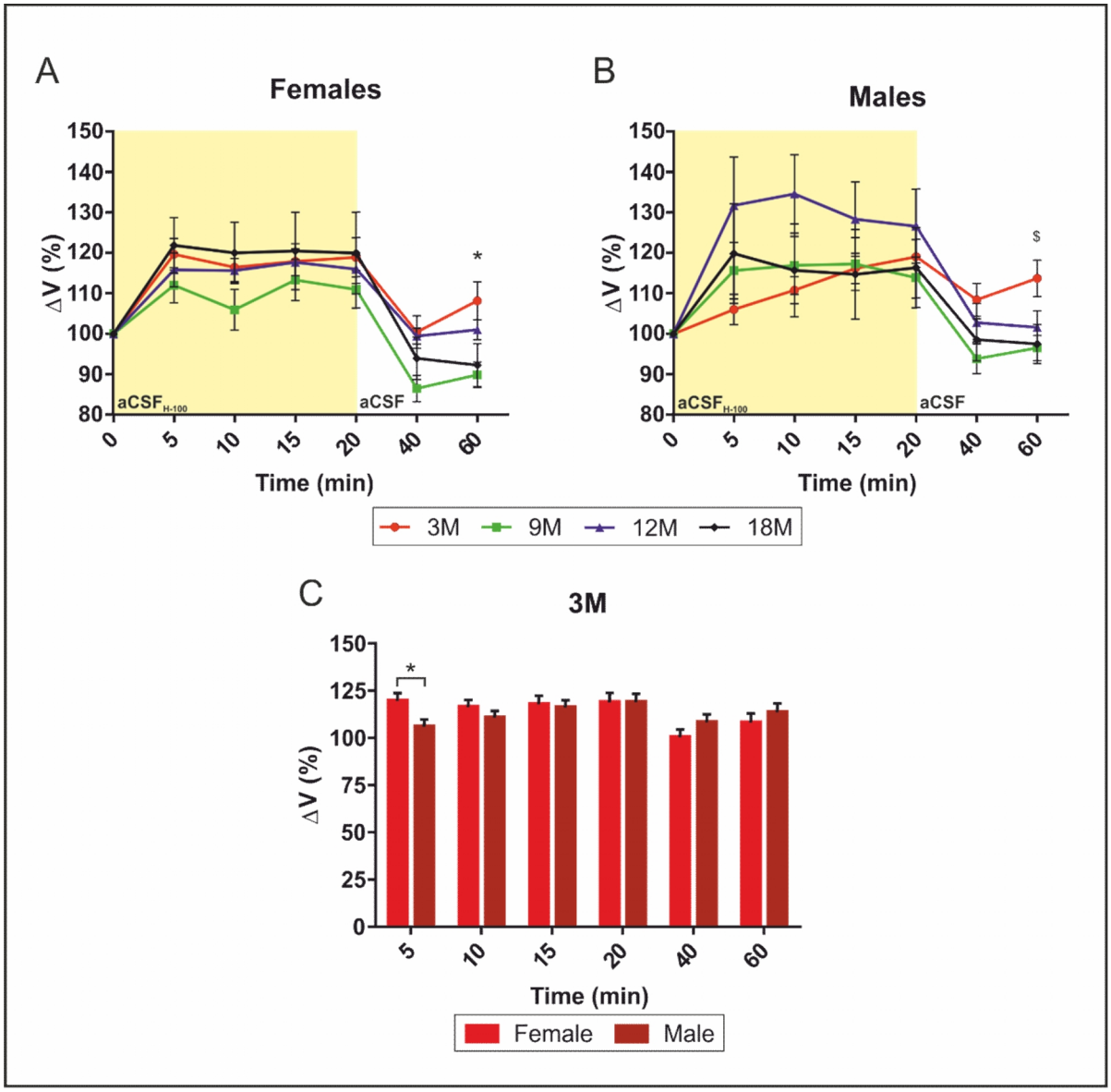

Figure 28: Astrocyte volume changes during hypotonic stress in different sexes. A+B: Time-dependent volume changes of astrocytes in female (A) and male (B) EGFP/GFAP mice from four age groups were recorded during the application of $aCSF_{H\text{-}100}$, followed by the application of aCSF. Data are given as percentage changes ± SEM. The original astrocyte volume is always shown as 100%. Asterisk indicates significant (*, $p<0.05$) difference between the volumes of female 3M and 18M astrocytes. Paragraph indicates significant ($, $p<0.05$) difference between the volumes of male 3M and 9M astrocytes. **C:** Percentage volume

changes + SEM of astrocytes from 3-month-old female and male mice induced by the 20-minute application of $aCSF_{H-100}$ followed by the wash-out with aCSF. Asterisk indicates the only significant (*, $p<0.05$) difference between male and female mice. 3M – 3-month-old mice; 9M – 9-month-old mice; 12M – 12-month-old mice; 18M – 18-month-old-mice; aCSF – artificial cerebrospinal fluid; $aCSF_{H-100}$ – hypotonic solution; SEM – standard error of the mean.

High response and low response astrocytes

Two subpopulations of astrocytes differing by the extent of their swelling during $aCSF_{H-100}$ application were identified in EGFP/GFAP mouse hippocampus and, based on previous studies (Benesova et al. 2009, 2012), cells whose total volume exceeded 110% at the 10^{th} minute of $aCSF_{H-100}$ application were termed high response (HR) astrocytes whereas the rest was termed low response (LR) astrocytes.

Looking at Figure 29, there is an obvious difference between LR and HR astrocytes. HR cells of all ages showed typical trend of the volume increase during $aCSF_{H-100}$ application and a decrease at first 20 minutes of wash-out. Once again, there was an increase of cell volume after 40 minutes of aCSF application in all age groups but 18M. At this final point of the wash-out, the only HR astrocyte significant difference was found between the volumes of 3M and 9M cells. LR astrocytes behaved differently. Their volume remained more or less steady during $aCSF_{H-100}$ application and the swelling, if present, was very mild. Volume changes during wash-out were comparable with what was described above. At first, there was a volume decrease, followed by an increase after 40 minutes, in this case in all four age groups. Statistically significant differences were found both after 20 and 40 minutes of aCSF application between 3M and 18M LR cells.

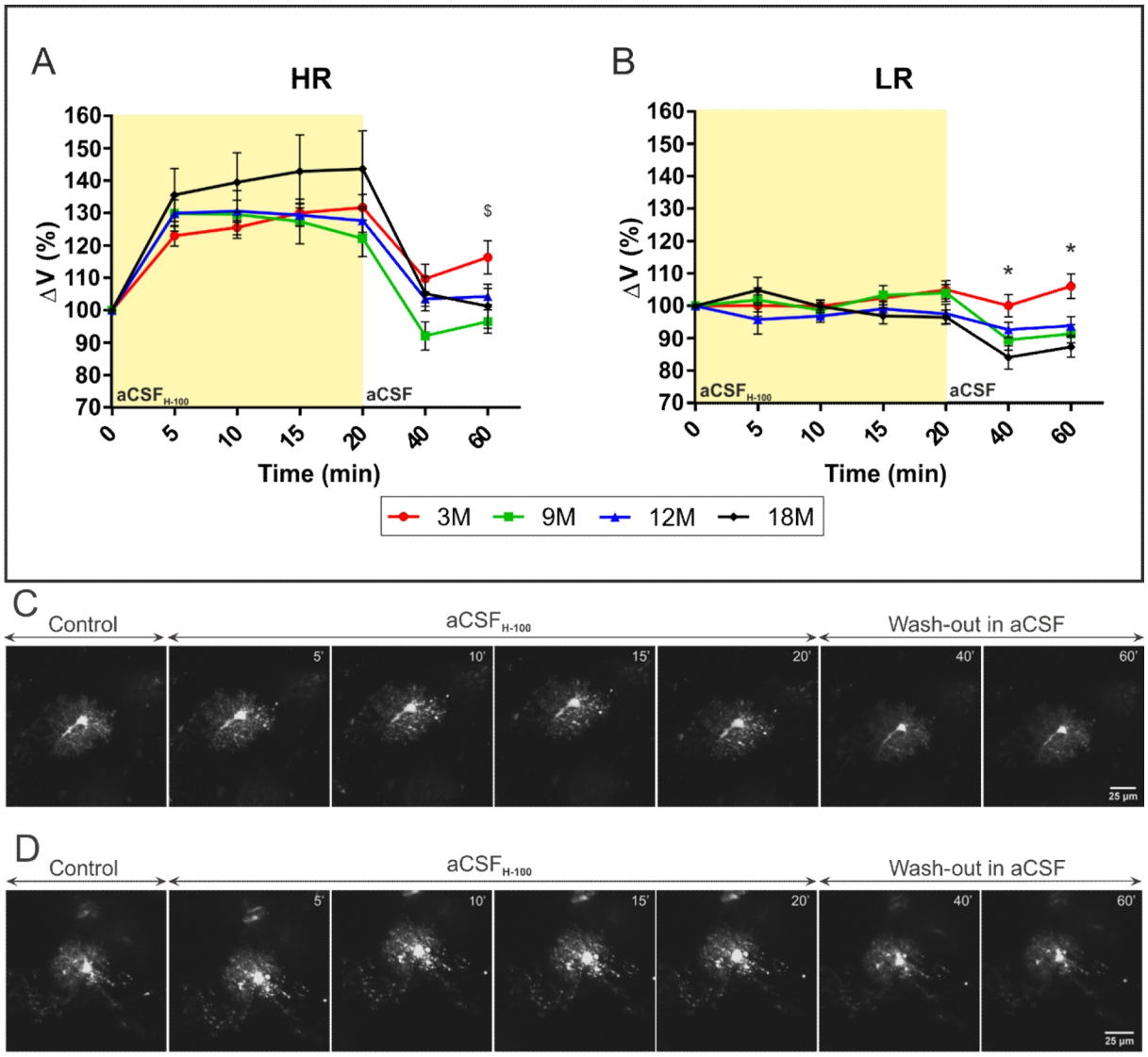

Figure 29: Volume changes of astrocytes from two different subpopulations. Two different subpopulations of astrocytes were distinguished during the experiment, low response and high response astrocytes. Time-dependent volume changes were measured for both groups during 20-minute application of $aCSF_{H-100}$, followed by the wash-out with aCSF and the data are given as percentage changes ± SEM. In all cases, the original volume is expressed as 100%. **A:** HR astrocytes present prominent swelling during the application of $aCSF_{H-100}$. Significant difference between the volumes of 3M and 9M HR astrocytes is represented by the paragraph ($, $p<0.05$). **B:** The volume of LR astrocytes is more or less constant during the application of both solutions. Asterisks indicate significant (*, $p<0.05$) differences between the volumes of 3M and 18M LR astrocytes. **C+D:** Superimposed images of LR astrocyte (C) and HR astrocyte (D) display their volumes at the beginning of the measurement (Control), during the $aCSF_{H-100}$ application and the aCSF wash-out. 3M – 3-month-old mice; 9M – 9-month-old mice; 12M – 12-month-old mice; 18M – 18-month-old-mice; aCSF – artificial cerebrospinal fluid; $aCSF_{H-100}$ – hypotonic solution, HR – high response; LR – low response; SEM – standard error of the mean.

In order to disclose whether the incidence of HR and LR astrocytes in mouse hippocampus changes with age, all the cells in each age group were counted and the numbers of HR and LR cells were expressed as a percentage of the total cell count (Figure 30). There is an obvious rise in the HR astrocyte numbers at 12M, however no significant differences were found between the incidences in different age groups.

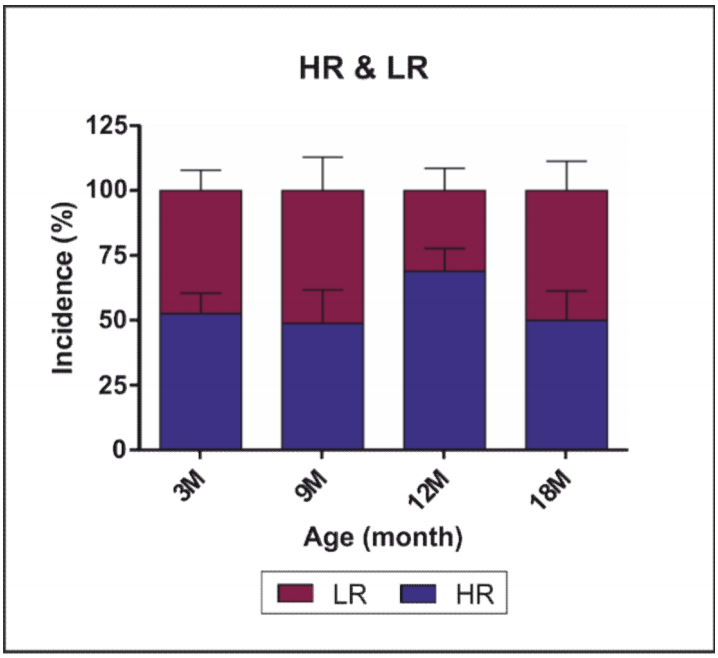

Figure 30: Incidence of high response and low response astrocytes in EGFP/GFAP mice of different age. After inspecting all the recorded cells, numbers of LR and HR astrocytes were acquired and given as percentage of the total number of the cells recorded during the experiment + SEM. Differences between the four age groups are not significant. 3M – 3-month-old mice; 9M – 9-month-old mice; 12M – 12-month-old mice; 18M – 18-month-old-mice; HR – high response; LR – low response; SEM – standard error of the mean.

High response and low response astrocytes in female and male EGFP/GFAP mice

HR and LR astrocytes are found equally in female and male mice. The data were evaluated separately for female and male cells to determine possible sex-dependent differences.

Typical swelling during $aCSF_{H\text{-}100}$ application was present in both female and male HR astrocytes (Figure 31A and C). After first 20 minutes of wash-out cells exhibited a decrease towards control values, followed by an increase in case of male 3M and 9M astrocytes and all female age groups but 18M. As seen at Figure 31A, female 18M astrocytes swelled to a greater extent than the rest of the age groups, however, it was not statistically significant. Similarly, no significant difference was found between the age groups in male

mice. Female and male HR astrocytes differed significantly only at the age of 12M after 10 minutes of $aCSF_{H\text{-}100}$ application, when the volume of male astrocytes reached significantly higher value (Figure 31E).

The volume of both female and male LR astrocytes remained more or less constant during the entire $aCFS_{H\text{-}100}$ application (Figure 31B and D). Mild volume decrease after the first 20 minutes of wash-out was followed by a small rise at 40th minute of the aCSF application in all age groups, both male and female. Male LR cells did not exhibit any significant difference between the age groups (Figure 31D). In female mice, LR astrocytes differed significantly during wash-out, after 40 minutes of aCSF application the swelling of 3M cells was significantly greater when compared with 9M and 18M cells. (Figure 31B). Significant differences during wash-out were also found between 12M male and female LR astrocytes (Figure 31F). No other sex-dependent differences of statistical significance were found.

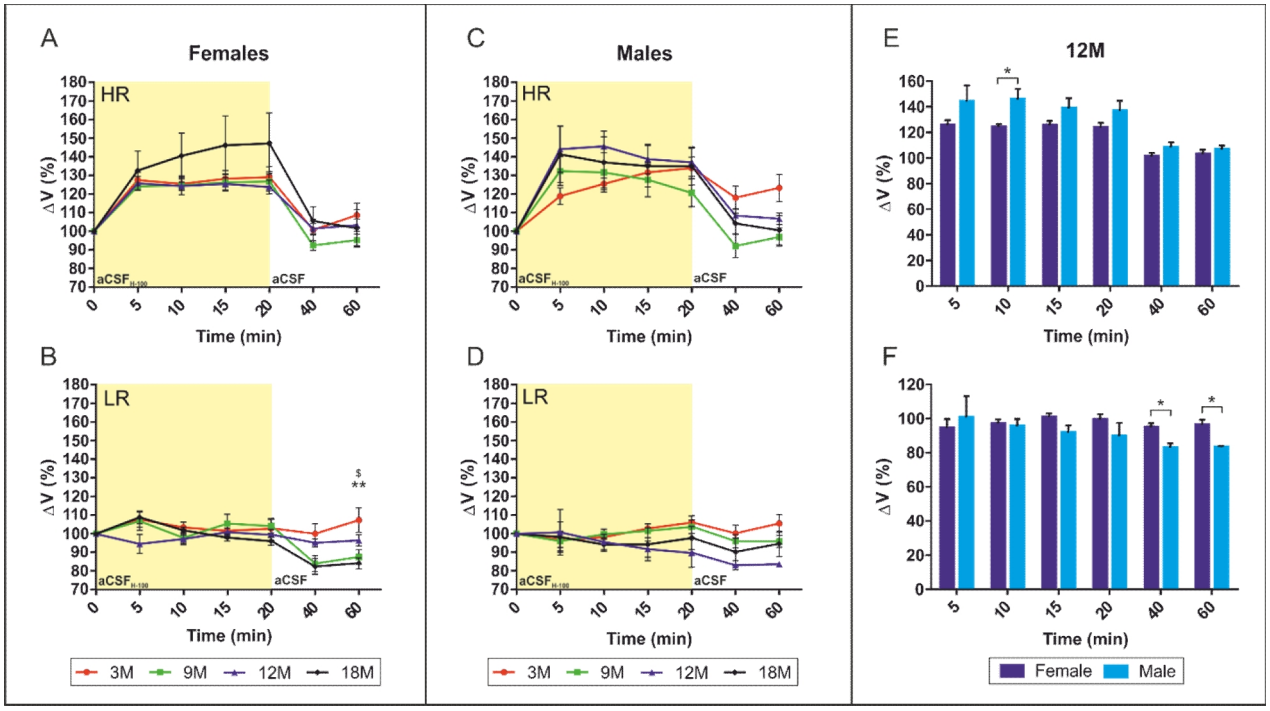

Figure 31: Time-dependent volume changes of astrocytes. Two different population of astrocytes were found in hippocampus of both female and male EGFP/GFAP mice. All the astrocyte volume changes were recorded during the 20-minute application of $aCSF_{H\text{-}100}$ followed by the 40-minute wash-out with aCSF. **A - D:** The data, evaluated separately for female HR (A) and LR (B) astrocytes and male HR (C) and LR (D) astrocytes, are given as percentage changes ± SEM. The original volume of astrocytes is always expressed as 100%. Both female and male HR astrocytes exhibit high extent of swelling during the $aCSF_{H\text{-}100}$ application, whereas the volume of LR astrocytes from both female and male EGFP/GFAP mice remains more or less constant. Asterisks indicate very significant (**, $p<0.01$) difference between the volumes of female 3M and 18M LR astrocytes.

Paragraph indicates significant ($, $p<0.05$) difference between the volumes of female 3M and 9M LR astrocytes. **E+F:** Volume changes of HR (E) and LR (F) astrocytes from 12-month-old female and male EGFP/GFAP mice are given as percentage changes + SEM. Asterisks indicate significant (*, $p<0.05$) differences found between female and male mice. 3M – 3-month-old mice; 9M – 9-month-old mice; 12M – 12-month-old mice; 18M – 18-month-old-mice; aCSF – artificial cerebrospinal fluid; $aCSF_{H-100}$ – hypotonic solution, HR – high response; LR – low response; SEM – standard error of the mean.

Incidence of LR and HR astrocytes was studied separately for male and female mice. There is a noteworthy decline in 9M female HR cells, but still not statistically significant. No significant difference between the four age groups was found in either females or males. Moreover, there was no statistically significant difference between the LR and HR incidences of female and male mice.

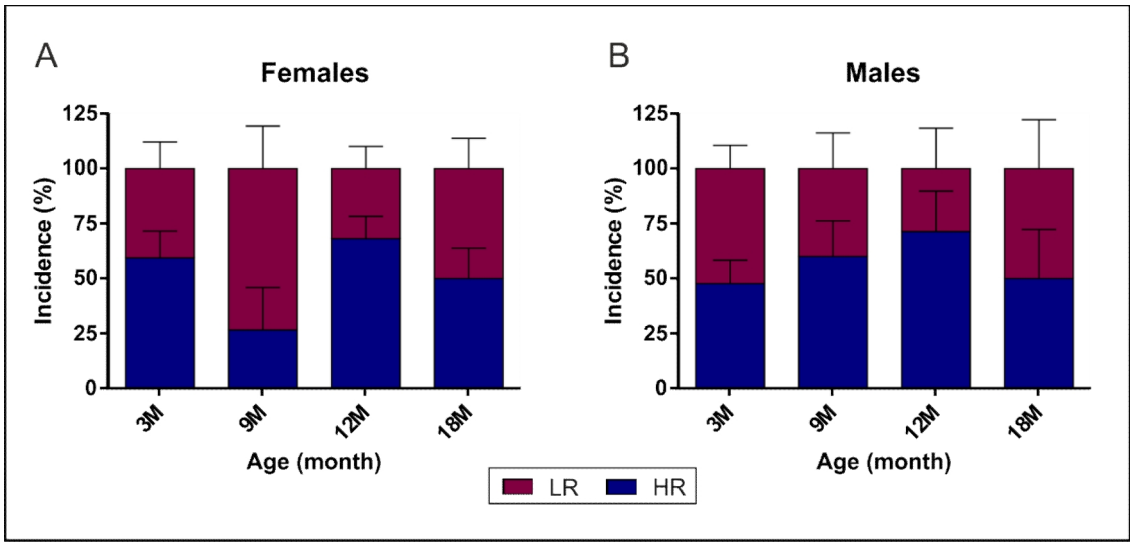

Figure 32: Incidence of high response and low response astrocytes. Numbers of LR and HR astrocytes for female (A) and male (B) EGFP/GFAP mice of different ages were acquired after examining all the cells measured in the experiment. They are given as percentage of the total number of the cells recorded during the experiment + SEM. Numbers of LR and HR astrocytes in both sexes show no significant difference between the four age groups. Likewise, no significant difference was discovered in the incidence of LR and HR astrocytes between female and male EGFP/GFAP mice. 3M – 3-month-old mice; 9M – 9-month-old mice; 12M – 12-month-old mice; 18M – 18-month-old-mice; HR – high response; LR – low response; SEM – standard error of the mean.

Discussion

We have demonstrated that astrocyte volume changes induced either by high extracellular K^+ concentration or by hypoosmotic stress vary with age and that two astrocyte subpopulations, differing in the extent of their swelling during application of hypoosmotic solution, exist in the EGFP/GFAP mouse hippocampus. However, we have not found any statistically significant difference when comparing incidence of these two subpopulations between the age groups or sexes. Additionally, some sex-dependent differences in astrocyte volume changes were discovered.

Astrocyte volume changes

During application of the solution with 50mM K^+, we have observed marked astrocyte swelling sometimes reaching considerably over 120%, followed by volume recovery. Similarly, astrocyte swelling was observed when hypoosmotic solution was applied, but the values hardly overcame 120%. Apparently, different channels and volume recovery mechanisms were put in use. Very comparable trends in volume changes were detected in the cortical astrocytes of EGFP/GFAP mice using both hypoosmotic solution and solution with high K^+ concentration (Anderova et al., 2014). Astrocyte swelling followed by volume recovery to various extent was observed in both cultured astrocytes and astrocytes *in situ* using various insults, such as oxygen/glucose deprivation, different hypoosmotic solutions and also solutions with different K^+ concentrations (Florence, Baillie, and Mulligan 2012). However, attempts to track astrocyte RVD *in vivo*, e.g. by using cranial window and two-photon laser scanning microscopy, were not successful, possibly because of the change in optical properties of swollen tissue or restricted duration of the experiment (Risher, Andrew, & Kirov, 2009)

When using $aCSF_{H\text{-}100}$ as the insult solution, age-dependent variations were present during wash-out when the volume should return near the original values. This volume recovery was the weakest in 3M astrocytes, implying that the RVD mechanisms are not fully developed yet. During $aCSF_{K+}$ application, the volume changes trend was same in all age groups however the extent of astrocyte swelling varied. Nonetheless, volume decrease during wash-out was evident in all age groups. Many of the astrocyte functions might be impaired by aging but it seems that volume recovery is not one of them. This is very important for the brain recovery after ischemia, when the K^+ extracellular concentration reaches easily 50mM, as it occurs more often among the elderly, when many astroglial neuroprotective functions

fails (Chisholm and Sohrabji 2015). When comparing neurons and astrocytes, the ability to recover volume is unique to astroglia. In opposite, e.g. during oxygen/glucose deprivation, neurons swell rapidly but are not capable to return their volume to the original value (Risher, Andrew, & Kirov, 2009).

Differences in the extent of the astrocyte swelling between the age groups might be explained by the changes in astrocyte physiology during aging. The expression of multiple channels involved in cell volume regulation differ with age. Aqp4, responsible for water influx and efflux, loses its perivascular localisation in aged brain (Kress et al. 2014) and this loss alters the volume regulating mechanisms, diminishing the range of astrocyte swelling (Anderova et al., 2014). This might be one of the reasons why the 18M astrocytes swell less than the 3M cells during $aCSF_{K+}$ application. Additionally, there are changes in cytoskeleton proteins such as GFAP that may lead to restricted swelling (Anderova et al., 2001). However, in hippocampus, GFAP levels rise with age (Rodríguez et al. 2014) and in contrary, it is the lack of GFAP that leads to limited swelling. Nonetheless, disturbances in GFAP and other cytoskeleton proteins influence also osmolyte fluxes, e.g. taurine efflux, which is important for RVD (Ding et al. 1998). Glutamate uptake is altered during aging as well and it was found in rat astrocyte cultures that especially female aged astrocytes are not able to clear the glutamate from media at the same rate as younger cells (Lewis et al. 2012). Moreover, gap junctions coupling is reduced in aged brain, causing impaired signalling within astroglia or deteriorating K^+ buffering, coupled with water transport (Cotrina et al. 2001).

Sex-dependent differences in astrocyte volume changes

We have found several differences between female and male astrocyte volume responses to various insults. Sex-dependent differences between volume changes during $aCSF_{H-100}$ application vary a lot and it is not possible to determine clear trend. However, when applying $aCSF_{K+}$, it seemed that male astrocytes tend to swell more than female cells, suggesting that female astrocytes have better RVD mechanisms. Completely opposite results were found when applying testosterone, estradiol and progesterone to the rat astrocyte culture. Na^+-K^+ ATPase pump, important part of RVD mechanisms, was stimulated by testosterone, but inhibited by both estradiol and progesterone, which supported volume increase (Fraser and Swanson 1994). When using mouse astrocytes, it was discovered that cultures from females were more resistant to oxygen/glucose deprivation than those from males. This difference disappeared when P450 aromatase inhibitor or knock-out mice were used. P450

aromatase is responsible for local synthesis of estrogen from testosterone, thus again implying role of sex hormones in volume regulation (Liu et al. 2008).

Volume changes in high response and low response astrocytes

Two subpopulations of astrocytes were discovered in EGFP/GFAP mouse hippocampus that react differently to hypoosmotic stress. High response astrocytes were swelling extensively, whereas low response cells kept constant volume and presented strong RVD mechanisms. These two subpopulations were observed before, in mouse cortex during hypotonic stress (Chvatal et al. 2007) or oxygen/glucose deprivation (Benesova et al. 2009). Similarly to these previous findings, we have seen that HR astrocytes increased their volume sharply during first minutes of the $aCSF_{H-100}$ application and remained swollen till the wash-out, while LR cells kept their volume near the original value during the entire application as a result of active RVD. RVD involves many ion channels, especially K^+ and Cl^- channels, Aqp4 and organic osmolyte efflux pathways (Hoffmann, Lambert, and Pedersen 2009) and differences in the expression of these channels and pathways might explain the different behaviour of the two astrocyte subpopulations. For example, gene for the ClC2 channel, activated by swelling, is highly expressed only in LR astrocytes, supporting their volume regulation. Additionally, striking difference was found in expression of channels from K_{2p} family, TWIK and TREK. While HR astrocytes express strongly TWIK-1 channel contributing to K^+ influx into the cell, LR astrocytes express TREK-1 channel, which enables K^+ efflux from the cells (Benesova et al. 2012). Difference between LR and HR astrocytes was discovered also between their ability to accumulate taurine, whose efflux plays essential role in RVD (Benesova et al. 2009). Another important component of cell volume regulation is NKCC co-transporter (Kahle et al. 2009), which was found to be expressed mainly in the processes of perivascular astrocytes, co-localizing with Aqp4 (Yan, Dempsey, and Sun 2001). The NKCC inhibitor caused marked reduction of swelling in mouse HR astrocytes, but did not have any effect on LR cells (Benesova et al. 2012), suggesting another difference between these two subpopulations. Additionally, age-dependent differences in the expression of this co-transporter were discovered in the rat brain, however the result from different studies varies, one implying a decline in the expression in the adulthood (Plotkin et al. 1997) while the other suggesting constant levels after the peak in the first month after birth (Yan, Dempsey, and Sun 2001). In our study, no age-dependent differences in both HR and LR astrocytes, that would be statistically significant, were found during $aCSF_{H-100}$ application. The volume increase in 18M HR astrocytes seemed to be greater than in younger cells,

however to confirm this trend, more measurements have to be performed on 18M mice. During wash-out, 3M astrocyte volume recovery was not as efficient as that of the older astrocytes, suggesting the corresponding mechanisms evolve with age.

The incidence of LR and HR astrocytes was same in all ages and sexes. As there was no statistically significant difference, we might speculate that none of the subpopulations is more susceptible to neuroinflammation and other pathologies associated with aging.

Conclusion

We have found some age-dependent differences in astrocyte volume regulation when applying both hypotonic solution and solution with high potassium concentrations. Two astrocyte subpopulations were identified based on their response to application of hypoosmotic solution. High response astrocytes presented marked swelling whereas low response astrocytes kept their volume steady. No difference in their incidence was found when comparing both age and sex.

Further research would be needed to determine e.g. what channels are responsible for the volume regulation and how is their expression changing with age.

Bibliography

Abbott, N. J., Rönnbäck, L., & Hansson, E. (2006). Astrocyte-endothelial interactions at the blood-brain barrier. *Nature Reviews. Neuroscience*, *7*(1), 41–53.

Aitken, P. G., Borgdorff, A. J., Juta, A. J. A., Kiehart, D. P., Somjen, G. G., & Wadman, W. J. (1998). Volume changes induced by osmotic stress in freshly isolated rat hippocampal neurons. *European Journal of Physiology*, *436*, 991–998.

Allansson, L., Khatibi, S., Gustavsson, T., Blomstrand, F., Olsson, T., & Hansson, E. (1999). Single-cell volume estimation by three-dimensional wide-field microscopy applied to astroglial primary cultures. *Journal of Neuroscience Methods*, *93*, 1–11.

Ambrosio, R. D., Gordon, D. S., Winn, H. R., Sepúlveda, F. V, Cid, L. P., Teulon, J., & Niemeyer, M. I. (2002). Differential Role of KIR Channel and Na + / K + -Pump in the Regulation of Extracellular K + in Rat Hippocampus. *Journal of Neurophysiology*, *87*, 87–102.

Amiry-Moghaddam, M., & Ottersen, O. P. (2003). The Molecular Basis of Water Transport in the Brain. *Nature Reviews. Neuroscience*, *4*, 991–1001.

Anderova, M., Benesova, J., Mikesova, M., Dzamba, D., Honsa, P., Kriska, J., … Vargova, L. (2014). Altered Astrocytic Swelling in the Cortex of α-Syntrophin-Negative GFAP/EGFP Mice. *PLoS ONE*, *9*, e113444.

Anderova, M., Kubinova, S., Mazel, T., Chvatal, A., Eliasson, C., Pekny, M., & Sykova, E. (2001). Effect of elevated K(+), hypotonic stress, and cortical spreading depression on astrocyte swelling in GFAP-deficient mice. *Glia*, *35*(3), 189–203.

Anderson, C. M., & Swanson, R. A. (2000). Astrocyte Glutamate Transport : Review of Properties , Regulation , and Physiological Functions. *Glia*, *32*, 1–14.

Aubert, S., Ebastien, S., Merle, M., Costalat, R., & Magistretti, P. J. (2007). Activity-Dependent Regulation of Energy Metabolism by Astrocytes : An Update. *Glia*, *55*, 1251–1262. doi:10.1002/glia

Ballanyi, B. Y. K., Grafe, P., & Bruggencate, G. T. E. N. (1987). Ion Activities and Potassium Uptake Mechanisms of Glial Cells in Guniea-Pig Olfacotry Cortex Slices. *Journal of Neurophysiology*, *382*, 159–174.

Barres, B. a. (2008). The mystery and magic of glia: a perspective on their roles in health and disease. *Neuron*, *60*(3), 430–40.

Benesova, J., Hock, M., Butenko, O., Prajerova, I., Anderova, M., & Chvatal, A. (2009). Quantification of Astrocyte Volume Changes During Ischemia In Situ Reveals Two Populations of Astrocytes in the Cortex of GFAP / EGFP Mice. *Journal of Neuroscience Research*, *87*(1), 96–111.

Benesova, J., Rusnakova, V., Honsa, P., Pivonkova, H., Dzamba, D., Kubista, M., & Anderova, M. (2012). Distinct expression/function of potassium and chloride channels contributes to the diverse volume regulation in cortical astrocytes of GFAP/EGFP mice. *PLoS ONE*, *7*(1), e29725.

Benfenati, V., & Ferroni, S. (2010). Water transport between CNS compartments: functional and molecular interactions between aquaporins and ion channels. *Neuroscience*, *168*(4), 926–40.

Bhat, R., Crowe, E. P., Bitto, A., Moh, M., Katsetos, C. D., Garcia, F. U., … Torres, C. (2012). Astrocyte senescence as a component of Alzheimer's disease. *PloS One*, *7*(9), e45069.

Blalock, E. M., Chen, K., Sharrow, K., Herman, J. P., Porter, N. M., Foster, T. C., & Landfield, P. W. (2003). Gene Microarrays in Hippocampal Aging : Statistical Profiling Identifies Novel Processes Correlated with Cognitive Impairment. *The Journal of Neuroscience*, *23*(9), 3807–3819.

Boudreault, F., & Grygorczyk, R. (2004). Evaluation of rapid volume changes of substrate-adherent cells by conventional microscopy 3D imaging. *Journal of Microscopy*, *215*, 302–312.

Brown, A. M., & Ransom, B. R. (2007). Astrocyte Glycogen and Brain Energy Metabolism. *Glia*, *55*, 1263–1271.

Brown, D. R. (2009). Role of microglia in age-related changes to the nervous system. *TheScientificWorldJournal*, *9*, 1061–1071.

Burger, T., Lucova, M., Moritz, R. E., Oelschläger, H. H. a, Druga, R., Burda, H., … Nemec, P. (2010). Changing and shielded magnetic fields suppress c-Fos expression in the navigation circuit: input from the magnetosensory system contributes to the internal representation of space in a subterranean rodent. *Journal of the Royal Society, Interface / the Royal Society*, *7*, 1275–1292.

Bushong, E. A., Martone, M. E., Jones, Y. Z., & Ellisman, M. H. (2002). Protoplasmic Astrocytes in CA1 Stratum Radiatum Occupy Separate Anatomical Domains. *The Journal of Neuroscience*, *22*(1), 183–192.

Cornell-Bell, A. H., Finkbeiner, S. M., Cooper, M. S., & Smith, S. J. (1990). Glutamate Induces Calcium Waves in Cultured Astrocytes: Long-Range Glial Signaling. *Science*, *247*(4941), 470–3.

Cotrina, M. L., Gao, Q., Lin, J. H. C., & Nedergaard, M. (2001). Expression and function of astrocytic gap junctions in aging. *Brain Research*, *901*, 55–61.

Cotrina, M. L., & Nedergaard, M. (2002). Astrocytes in the Aging Brain. *Journal of Neuroscience Research*, *67*, 1–10.

Crowe, W. E., Altamirano, J., Huerto, L., & Alvarez-Leefmans, F. J. (1995). Volume Changes in Single N1E-115 Neuroblastoma Cells With a Fluorescent Probe. *Neuroscience*, *69*(1), 283–296.

Danbolt, N. C. (2001). Glutamate uptake. *Progress in Neurobiology*, *65*, 1–105.

Davis, C. E., Rychak, J. J., Hosticka, B., Davis, S. C., John III, J. E., Tucker, A. L., … Moorman, J. R. (2004). A novel method for measuring dynamic changes in cell volume. *Journal of Applied Physiology*, *96*, 1886–1893.

Dermietzel, R., & Spray, D. C. (1993). Gap jundions in the brain : where , what type , how many and why ? *Trends in Neurosciences*, *16*(5), 186–92.

Ding, M., Eliasson, C., Betsholtz, C., Hamberger, A., & Pekny, M. (1998). Altered taurine release following hypotonic stress in astrocytes from mice deficient for GFAP and vimentin. *Molecular Brain Research*, *62*(1), 77–81.

Doupnik, C. A., Davidson, N., & Lester, H. A. (1995). The inward rectifier potassium channel family. *Current Opinion in Neurobiology*, *5*, 268–277.

Eng, L. F., Ghirnikar, R. S., & Lee, Y. L. (2000). Glial Fibrillary Acidic Protein : GFAP-Thirty-One Years (1969 – 2000)*. *Neurochemical Research*, *25*(9-10), 1439–1451.

Eroglu, C., & Barres, B. (2010). Regulation of synaptic connectivity by glia. *Nature*, *468*, 223–231.

Esiri, M. M. (2007). Ageing and the brain. *The Journal of Pathology*, *211*(2), 181–7.

Fabricius, K., Jacobsen, J. S., & Pakkenberg, B. (2013). Effect of age on neocortical brain cells in 90+ year old human females--a cell counting study. *Neurobiology of Aging*, *34*(1), 91–9.

Fellin, T., Pascual, O., Gobbo, S., Pozzan, T., Haydon, P. G., Carmignoto, G., … Walk, H. (2004). Neuronal Synchrony Mediated by Astrocytic Glutamate through Activation of Extrasynaptic NMDA Receptors. *Neuron*, *43*, 729–743.

Finch, C. E. (2003). Neurons, glia, and plasticity in normal brain aging. *Neurobiology of Aging*, *24*, S123–S127.

Florence, C. M., Baillie, L. D., & Mulligan, S. J. (2012). Dynamic Volume Changes in Astrocytes Are an Intrinsic Phenomenon Mediated by Bicarbonate Ion Flux. *PLoS ONE*, *7*(11), 1–9.

Fraser, C. L., & Swanson, R. (1994). Female sex hormones inhibit volume regulation in rat brain astrocyte culture. *The American Journal of Physiolog*, *267*, 909–14.

Giaume, C., & Venance, L. (1998). Intercellular Calcium Signaling and Gap Junctional Communication in Astrocytes. *Glia*, *24*, 50–64.

Gonçalves, C.-A., Leite, M. C., & Nardin, P. (2008). Biological and methodological features of the measurement of S100B, a putative marker of brain injury. *Clinical Biochemistry*, *41*(10-11), 755–63.

Gray, D. a, & Woulfe, J. (2005). Lipofuscin and aging: a matter of toxic waste. *Science of Aging Knowledge Environment : SAGE KE*, *2005*(5), re1.

Grosche, A., Grosche, J., Tackenberg, M., Scheller, D., Gerstner, G., Gumprecht, A., … Reichenbach, A. (2013). Versatile and Simple Approach to Determine Astrocyte Territories in Mouse Neocortex and Hippocampus. *PloS One*, *8*(7), e69143.

Haas, M., & Forbush, B. I. (1998). The Na-K-Cl Cotransporters. *Journal of Bioenergetics and Biomembranes*, *30*(2), 161–173.

Halassa, M. M., Fellin, T., & Haydon, P. G. (2007). The tripartite synapse : roles for gliotransmission in health and disease. *Trends in Molecular Medicine*, *13*(2), 54–63.

Halassa, M. M., Fellin, T., Takano, H., Dong, J.-H., & Haydon, P. G. (2007). Synaptic islands defined by the territory of a single astrocyte. *The Journal of Neuroscience : The Official Journal of the Society for Neuroscience*, *27*(24), 6473–7.

Hama, K., Arii, T., Katayama, E., Marton, M., & Ellisman, M. H. (2004). Tri-dimensional morphometric analysis of astrocytic processes with high voltage electron microscopy of thick Golgi preparations. *Journal of Neurocytology*, *33*, 277–285.

Heneka, M. T., Rodríguez, J. J., & Verkhratsky, A. (2010). Neuroglia in neurodegeneration. *Brain Research Reviews*, *63*(1-2), 189–211.

Hirrlinger, P. G., Wurm, A., Hirrlinger, J., Bringmann, A., & Reichenbach, A. (2008). Osmotic swelling characteristics of glial cells in the murine hippocampus, cerebellum, and retina in situ. *Journal of Neurochemistry*, *105*, 1405–1417.

Hoffmann, E. K., Lambert, I. H., & Pedersen, S. F. (2009). Physiology of cell volume regulation in vertebrates. *Physiological Reviews*, *89*(1), 193–277.

Chisholm, N. C., & Sohrabji, F. (2015). Astrocytic response to cerebral ischemia is influenced by sex differences and impaired by aging. *Neurobiology of Disease*.

Chvatal, A., Anderova, M., Hock, M., Prejova, I., Neprasova, H., Chvatal, V., … Sykova, E. (2007). Three-Dimensional Confocal Morphometry Reveals Structural Changes in Astrocyte Morphology In Situ. *Journal of Neuroscience Research*, *85*, 260–271.

Chvatal, A., Anderova, M., & Kirchhoff, F. (2007). Three-dimensional confocal morphometry - a new approach for studying dynamic changes in cell morphology in brain slices. *Journal of Anatomy*, *210*(6), 671–83.

Iadecola, C., & Nedergaard, M. (2007). Glial regulation of the cerebral microvasculature. *Nature Neuroscience*, *10*(11), 1369–1376.

Jabs, R., Matthias, K., Grote, A., Grauer, M., & Seifert, G. (2007). Lack of P2X Receptor Mediated Currents in Astrocytes and GluR Type Glial Cells of the Hippocampal CA1 Region. *Glia*, *55*, 1648–1655.

Jacobs, B. O. B., Driscoll, L., & Schall, M. (1997). Life-Span Dendritic and Spine Changes in Areas 10 and 18 of Human Cortex: A Quantitative Golgi Study. *The Journal of Comparative Neurology*, *386*, 661–680.

Jung, J. S., Bhat, R. V, Preston, G. M., Guggino, W. B., Baraban, J. M. & Agre, P. (1994). Molecular characterization of an aquaporin cDNA from brain : Candidate osmoreceptor and regulator of water balance. *Proceedings of the National Academy of Science of the United States of Amercia*, *91*, 13052–13056.

Kahle, K. T., Simard, J. M., Staley, K. J., Nahed, B. V, Jones, P. S., & Sun, D. (2009). Molecular mechanisms of ischemic cerebral edema: role of electroneutral ion transport. *Physiology*, *24*, 257–265.

Kaplan, J. H. (2002). Biochemistry of Na,K-ATPase. *Annual Review of Biochemistry*, *71*, 511–35.

Kimelberg, H. K. (2005). Astrocytic Swelling in Cerebral Ischemia As a Possible Cause of Injury and Target for Therapy. *Glia*, *50*, 389–397.

Kimelberg, H. K., Macvicar, B. A., & Sontheimer, H. (2006). Anion Channels in Astrocytes: Biophysics, Pharmacology, and Function. *Glia*, *54*(7), 747–757.

Knepper, M. A. (1994). The aquaporin family of molecular water channels. *Proceedings of the National Academy of Science of the United States of Amercia*, *91*(14), 6255–6258.

Kofuji, P., & Newman, E. a. (2004). Potassium buffering in the central nervous system. *Neuroscience*, *129*(4), 1045–56.

Korchev, Y. E., Gorelik, J., Sviderskaya, E. V, Johnston, C. L., Coombes, C. R., Vodyanoy, I., & Edwards, C. R. W. (2000). Cell Volume Measurement Using Scanning Ion Conductance Microscopy. *Biophysical Journal*, *78*, 451–457.

Kress, B. T., Iliff, J. J., Xia, M., Wang, M., Wei, H. S., Zeppenfeld, D., … Nedergaard, M. (2014). Impairment of Paravascular Clearance Pathways in the Aging Brain. *Annals of Neurology*, *76*, 845–861.

Lalo, U., Palygin, O., North, R. A., Verkhratsky, A., & Pankratov, Y. (2011). Age-dependent remodeling of ionotropic signalling in cortical astroglia. *Aging Cell*, *10*, 392–402.

Lalo, U., Pankratov, Y., Wichert, S. P., Rossner, M. J., North, R. A., Kirchhoff, F., & Verkhratsky, A. (2008). P2X 1 and P2X 5 Subunits Form the Functional P2X Receptor in Mouse Cortical Astrocytes. *The Journal of Neuroscience*, *28*(21), 5473–5480.

Lang, F., Busch, G. L., Ritter, M., Vo, H., Waldegger, S., & Gulbins, E. (1998). Functional Significance of Cell Volume Regulatory Mechanisms. *Physiological Reviews*, *78*(1), 247–307.

Lewis, D. K., Thomas, K. T., Selvamani, A., & Sohrabji, F. (2012). Age-related severity of focal ischemia in female rats is associated with impaired astrocyte function. *Neurobiology of Aging*, *33*(6), 1123.e1–1123.e16.

Liu, M., Oyarzabal, E., Yang, R., Murphy, S. J., & Hurn, P. D. (2008). A Novel Method for Assessing Sex-Specific and Genotype- Specific Response to Injury in Astrocyte Culture. *Journal of Neuroscience Methods*, *171*(2), 214–217.

Lutz, S. E., Zhao, Y., Gulinello, M., Lee, S. C., Raine, C. S., & Brosnan, C. F. (2009). Deletion of Astrocyte Connexin 43 and 30 Leads to a Dysmyelinating Phenotype and Hippocampal CA1 Vacuolation. *The Journal of Neuroscience*, *29*(24), 7743–7752.

Lynch, A. M., Murphy, K. J., Deighan, B. F., Reilly, J. O., Gun, Y. K., Cowley, T. R., … Lynch, M. A. (2010). The Impact of Glial Activation in the Aging Brain. *Aging and Disease*, *1*(3), 262–278.

MacAulay, N., Hamann, S., & Zeuthen, T. (2004). Water transport in the brain: role of cotransporters. *Neuroscience*, *129*(4), 1031–44.

Macvicar, B. A., Feighan, D., Brown, A., & Ransom, B. (2002). Intrinsic Optical Signals in the Rat Optic Nerve : Role for K+ Uptake via NKCC1 and Swelling of Astrocytes. *Glia*, *37*, 114–123.

Matthias, K., Kirchhoff, F., Seifert, G., Hüttmann, K., Matyash, M., Kettenmann, H., & Steinhäuser, C. (2003). Segregated expression of AMPA-type glutamate receptors and glutamate transporters defines distinct astrocyte populations in the mouse hippocampus. *The Journal of Neuroscience : The Official Journal of the Society for Neuroscience*, *23*(5), 1750–1758.

McCall, M. A., Gregg, R. G., Behringer, R. R., Brenner, M., Delaney, C. L., Galbreath, E. J., … Messing, A. (1996). Targeted deletion in astrocyte intermediate filament (Gfap) alters neuronal physiology. *Proceedings of the National Academy of Science of the United States of Amercia*, *93*, 6361–6366.

McTigue, D. M., & Tripathi, R. B. (2008). The life, death, and replacement of oligodendrocytes in the adult CNS. *Journal of Neurochemistry*, *107*(1), 1–19.

Menet, V., Gimenez Y Ribotta, M., Sandillon, F., & Privat, A. (2000). GFAP Null Astrocytes Are a Favorable Substrate for Neuronal Survival and Neurite Growth. *Glia*, *31*, 267–272.

Messing, A., Head, M. W., Galles, K., Galbreath, E. J., Goldman, J. E., & Brenner, M. (1998). Fatal Encephalopathy with Astrocyte Inclusions in GFAP Transgenic Mice. *American Journal of Pathology*, *152*(2), 391–398.

Mulligan, S. J., & Macvicar, B. A. (2004). Calcium transients in astrocyte endfeet cause cerebrovascular constrictions. *Nature*, *431*(7005), 195–9.

Nedergaard, M., Ransom, B., & Goldman, S. a. (2003). New roles for astrocytes: redefining the functional architecture of the brain. *Trends in Neurosciences*, *26*(10), 523–30.

Nielsen, S., Nagelhus, E. A., Amiry-moghaddam, M., Bourque, C., Agre, P., & Ottersen, O. P. (1997). Specialized Membrane Domains for Water Transport in Glial Cells : High-Resolution Immunogold Cytochemistry of Aquaporin-4 in Rat Brain. *The Journal of Neuroscience*, *17*(1), 171–180.

Njie, Em. G., Boelenb, E., R., S. F., Steinbusch, Ha. W. M., Borchelt, D. R., & Streit, W. J. (2012). Ex vivo cultures of microglia from young and aged rodent brain reveal age-related changes in microglial function. *Neurobiology of Aging*, *33*(1), 195.e1–12.

Nolte, C., Matyash, M., Pivneva, T., Schipke, C. G., Ohlemeyer, C., Hanisch, U., & Delbru, M. (2001). GFAP Promoter-Controlled EGFP- Expressing Transgenic Mice : A Tool to Visualize Astrocytes and Astrogliosis in Living Brain Tissue. *Glia*, *33*, 72–86.

Norden, D. M., & Godbout, J. P. (2013). Review: Microglia of the aged brain: Primed to be activated and resistant to regulation. *Neuropathology and Applied Neurobiology*, *39*, 19–34.

Norenberg, D. (1979). The Distribution of Glutamine Synthetase in the Rat Central Nervous System. *The Journal of Histochemistry and Cytochemistry*, *27*(3), 756–762.

Oberheim, N. A., Takano, T., Han, X., He, W., Lin, J. H. C., Xu, Q., … Nedergaard, M. (2009). Uniquely hominid features of adult human astrocytes. *The Journal of Neuroscience*, *29*(10), 3276–87.

Ogata, K., & Kosaka, T. (2002). Structural and quantitative analysis of astrocytes in the mouse hippocampus. *Neuroscience*, *113*(1), 221–233.

Pakkenberg, B., & Gundersen, H. J. G. (1997). Neocortical Neuron Number in Humans : Effect of Sex and Age. *The Journal of Comparative Neurology*, *384*, 312–320.

Pampaloni, F., Reynaud, E. G., & Stelzer, E. H. K. (2007). The third dimension bridges the gap between cell culture and live tissue. *Nature Reviews. Molecular Cell Biology*, *8*, 839–845.

Pannese, E. (2013). Neuroglial cells: morphological changes during normal aging. *Rendiconti Lincei*, *24*(2), 101–106.

Pannicke, T., Wurm, A., Iandiev, I., Hollborn, M., Linnertz, R., Binder, D. K., … Bringmann, A. (2010). Deletion of aquaporin-4 renders retinal glial cells more susceptible to osmotic stress. *Journal of Neuroscience Research*, *88*, 2877–2888.

Parpura, V., Basarsky, T., Liu, F., & Jeftinija, K. (1994). Glutamate-mediated astrocyte–neuron signalling. *Nature*, *369*, 744–747.

Pascual, O., Casper, K. B., Kubera, C., Zhang, J., Revilla-sanchez, R., Sul, J., … Haydon, P. G. (2005). Astrocytic Purinergic Signaling Coordinates Synaptic Networks. *Science*, *310*, 113–116.

Pekny, M., & Nilsson, M. (2005). Astrocyte activation and reactive gliosis. *Glia*, *50*(4), 427–34. doi:10.1002/glia.20207

Pekny, M., & Pekna, M. (2004). Astrocyte intermediate filaments in CNS pathologies and regeneration. *The Journal of Pathology*, *204*(4), 428–37.

Pekny, M., Wilhelmsson, U., & Pekna, M. (2014). The dual role of astrocyte activation and reactive gliosis. *Neuroscience Letters*, *565*, 30–8.

Pelvig, D. P., Pakkenberg, H., Stark, a K., & Pakkenberg, B. (2008). Neocortical glial cell numbers in human brains. *Neurobiology of Aging*, *29*(11), 1754–62.

Pérez-Alvarez, A., Araque, A., & Martín, E. D. (2013). Confocal microscopy for astrocyte in vivo imaging: Recycle and reuse in microscopy. *Frontiers in Cellular Neuroscience*, *7*(April), 51.

Peters, A., & Sethares, C. (2004). Oligodendrocytes, their progenitors and other neuroglial cells in the aging primate cerebral cortex. *Cerebral Cortex*, *14*(September), 995–1007.

Pines, G., Danbolt, N. C., Bjørås, M., Zhang, Y., Bendahan, a, Eide, L., … Kanner, B. I. (1992). Cloning and expression of a rat brain L-glutamate transporter. *Nature*, *360*, 464–467.

Plotkin, M. D., Snyder, E. Y., Hebert, S. C., & Delpire, E. (1997). Expression of the Na-K-2Cl cotransporter is developmentally regulated in postnatal rat brains: A possible mechanism underlying GABA's excitatory role in immature brain. *Journal of Neurobiology*, *33*, 781–795.

Popescu, B. O., Toescu, E. C., Popescu, L. M., Bajenaru, O., Muresanu, D. F., Schultzberg, M., & Bogdanovic, N. (2009). Blood-brain barrier alterations in ageing and dementia. *Journal of the Neurological Sciences*, *283*(1-2), 99–106.

Powell, E. M., & Geller, H. M. (1999). Dissection of Astrocyte-Mediated Cues in Neuronal Guidance and Process Extension. *Glia*, *26*, 73–83.

Ransohoff, R. M., & Perry, V. H. (2009). Microglial physiology: unique stimuli, specialized responses. *Annual Review of Immunology*, *27*, 119–45.

Ransom, C. B., Ransom, B. R., & Sontheimer, H. (2000). Activity-dependent extracellular K+ accumulation in rat optic nerve : the role of glial and axonal Na+ pumps. *Journal of Physiology*, *522*(3), 427–442.

Raz, N., & Rodrigue, K. M. (2006). Differential aging of the brain: patterns, cognitive correlates and modifiers. *Neuroscience and Biobehavioral Reviews*, *30*(6), 730–48.

Ringel, F., & Plesnila, N. (2008). Expression and functional role of potassium-chloride cotransporters (KCC) in astrocytes and C6 glioma cells. *Neuroscience Letters*, *442*, 219–223.

Risher, W. C., Andrew, R. D., & Kirov, S. A. (2009a). Real-Time Passive Volume Responses of Astrocytes to Acute Osmotic and Ischemic Stress in Cortical Slices and in vivo Revealed by Two-Photon Microscopy. *Glia*, *57*(2), 207–221.

Risher, W. C., Andrew, R. D., & Kirov, S. a. (2009b). Real-time passive volume responses of astrocytes to acute osmotic and ischemic stress in cortical slices and in vivo revealed by two-photon microscopy. *Glia*, *57*, 207–221.

Rodríguez, J. J., Yeh, C.-Y., Terzieva, S., Olabarria, M., Kulijewicz-Nawrot, M., & Verkhratsky, A. (2014). Complex and region-specific changes in astroglial markers in the aging brain. *Neurobiology of Aging*, *35*(1), 15–23.

Rodríguez-Arellano, J. J., Parpura, V., Zorec, R., & Verkhratsky, a. (2015). Astrocytes in physiological aging and Alzheimer's disease. *Neuroscience*.

Rouach, N., Koulakoff, A., Abudara, V., Willecke, K., & Giaume, C. (2008). Astroglial Metabolic Networks Sustain Hippocampal Synaptic Transmission. *Science*, *322*(5907), 1551–1555.

Rutten, B. (2003). The aging brain: less neurons could be better. *Mechanisms of Ageing and Development*, *124*(3), 349–355.

Salminen, A., Ojala, J., Kaarniranta, K., Haapasalo, A., Hiltunen, M., & Soininen, H. (2011). Astrocytes in the aging brain express characteristics of senescence-associated secretory phenotype. *The European Journal of Neuroscience*, *34*(1), 3–11.

Scemes, E., & Giaume, C. (2006). Astrocyte Calcium Waves: What They Are and What They Do. *Glia*, *54*(7), 716–725.

Seifert, G., Schilling, K., & Steinhäuser, C. (2006). Astrocyte dysfunction in neurological disorders: a molecular perspective. *Nature Reviews. Neuroscience*, *7*, 194–206.

Siemkowicz, E., & Hansen, a J. (1981). Brain extracellular ion composition and EEG activity following 10 minutes ischemia in normo- and hyperglycemic rats. *Stroke; a Journal of Cerebral Circulation*, *12*(2), 236–240.

Simard, M., & Nedergaard, M. (2004). The neurobiology of glia in the context of water and ion homeostasis. *Neuroscience*, *129*(4), 877–96.

Simic, G., Kostovic, I., Winblad, B., & Bogdanovic, N. (1997). Volume and Number of Neurons of the Human Hippocampal Formation in Normal Aging and Alzheimer ' s Disease. *The Journal of Comparative Neurology*, *379*, 482–494.

Sofroniew, M. V, & Vinters, H. V. (2010). Astrocytes: biology and pathology. *Acta Neuropathologica*, *119*(1), 7–35.

Somjen, G. G. (2004). *Ions in the brain: Normal function, Seizures, and Stroke*. Oxford University Press, Oxford, UK.

Stevens, B., Allen, N. J., Vazquez, L. E., Howell, G. R., Christopherson, K. S., Nouri, N., … Barres, B. a. (2007). The classical complement cascade mediates CNS synapse elimination. *Cell*, *131*(6), 1164–78.

Storck, T., Schulte, S., Hofmann, K., & Stoffel, W. (1992). Structure, expression, and functional analysis of a Na(+)-dependent glutamate/aspartate transporter from rat brain. *Proceedings of the National Academy of Sciences of the United States of America*, *89*(November), 10955–10959.

Streit, W. J., Sammons, N. W., Kuhns, A. J., & Sparks, D. L. (2004). Dystrophic Microglia in the Aging Human Brain. *Glia*, *45*, 208–212.

Sulzer, D., Mosharov, E., Talloczy, Z., Zucca, F. a, Simon, J. D., & Zecca, L. (2008). Neuronal pigmented autophagic vacuoles: lipofuscin, neuromelanin, and ceroid as macroautophagic responses during aging and disease. *Journal of Neurochemistry*, *106*(1), 24–36.

Swanson, L., Araque, A., Parpura, V., Sanzgiri, R. P., & Haydon, P. G. (1999). Tripartite synapses : glia , the unacknowledged partner. *Trends in Neurosciences*, *22*(5), 208–15.

Torres-Platas, S. G., Hercher, C., Davoli, M. A., Maussion, G., Labonté, B., Turecki, G., & Mechawar, N. (2011). Astrocytic Hypertrophy in Anterior Cingulate White Matter of Depressed Suicides. *Neuropsychopharmacology*, *36*, 2650–2658.

Ullian, E. M., Sapperstein, S. K., Christopherson, K. S., & Barres, B. A. (2001). Control of Synapse Number by Glia. *Science*, *291*(5504), 657–61.

Verkhratsky, A., & Kettenmann, H. (1996). Calcium signaling in glial cells. *Trends in Neurosciences*, *19*(8), 346–52.

Verkhratsky, A., Olabarria, M., Noristani, H. N., Yeh, C., & Rodriguez, J. J. (2010). Astrocytes in Alzheimer ' s Disease. *Neurotherapeutics*, *7*, 399–412.

Verkhratsky, A., & Steinhauser, C. (2000). Ion channels in glial cells. *Brain Research Reviews*, *32*, 380–412.

Watts, L. T., & Lechleiter, J. D. (2009). Physiological Changes in Astrocytes During Aging Cell. In: *Astrocytes in (Patho)Physiology of the Nervous System,* Haydon, P. G. & Parpura, V. (eds), Springer, Boston, Massachusetts, USA, pp. 569–590.

Yan, Y., Dempsey, R. J., & Sun, D. (2001). Expression of Na+-K+-Cl- cotransporter in rat brain during development and its localization in mature astrocytes. *Brain Research*, *911*, 43–55.

Zeevi, N., Pachter, J., McCullough, L. D., Wolfson, L., & Kuchel, G. a. (2010). The blood-brain barrier: geriatric relevance of a critical brain-body interface. *Journal of the American Geriatrics Society*, *58*(9), 1749–57.

Zonta, M., Angulo, M. C., Gobbo, S., Rosengarten, B., Hossmann, K., Pozzan, T., & Carmignoto, G. (2003). Neuron-to-astrocyte signaling is central to the dynamic control of brain microcirculation. *Nature Neuroscience*, *6*(1), 43–50.

Zoremba, N., Homola, A., Slais, K., Vorísek, I., Rossaint, R., Lehmenkühler, A., & Syková, E. (2008). Extracellular diffusion parameters in the rat somatosensory cortex during

recovery from transient global ischemia/hypoxia. *Journal of Cerebral Blood Flow and Metabolism : Official Journal of the International Society of Cerebral Blood Flow and Metabolism*, *28*, 1665–1673.